# Branch cuts of Stokes wave on deep water. Part I: Numerical solution and Padé approximation

**Sergey A. Dyachenko**[1,2]**, Pavel M. Lushnikov**[3,4]†**,**
**and Alexander O. Korotkevich**[3,4]

[1]Department of Mathematics, University of Illinois at Urbana-Champaign, 1409 W. Green Street, Urbana, IL 61801, USA

[2]Department of Mathematics, University of Arizona, 617 N. Santa Rita Ave., P.O. Box 210089, Tucson, AZ 85721, USA

[3]Department of Mathematics and Statistics, University of New Mexico, Albuquerque, MSC01 1115, NM, 87131, USA

[4]Landau Institute for Theoretical Physics, 2 Kosygin Str., Moscow, 119334, Russia

Complex analytical structure of Stokes wave for two-dimensional potential flow of the ideal incompressible fluid with free surface and infinite depth is analyzed. Stokes wave is the fully nonlinear periodic gravity wave propagating with the constant velocity. Simulations with the quadruple (32 digits) and variable precisions (more than 200 digits) are performed to find Stokes wave with high accuracy and study the Stokes wave approaching its limiting form with $2\pi/3$ radians angle on the crest. A conformal map is used which maps a free fluid surface of Stokes wave into the real line with fluid domain mapped into the lower complex half-plane. The Stokes wave is fully characterized by the complex singularities in the upper complex half-plane. These singularities are addressed by rational (Padé) interpolation of Stokes wave in the complex plane. Convergence of Padé approximation to the density of complex poles with the increase of the numerical precision and subsequent increase of the number of approximating poles reveals that the only singularities of Stokes wave are branch points connected by branch cuts. The converging densities are the jumps across the branch cuts. There is one branch cut per horizontal spatial period $\lambda$ of Stokes wave. Each branch cut extends strictly vertically above the corresponding crest of Stokes wave up to complex infinity. The lower end of branch cut is the square-root branch point located at the distance $v_c$ from the real line corresponding to the fluid surface in conformal variables. The increase of the scaled wave height $H/\lambda$ from the linear limit $H/\lambda = 0$ to the critical value $H_{max}/\lambda$ marks the transition from the limit of almost linear wave to a strongly nonlinear limiting Stokes wave (also called by the Stokes wave of the greatest height). Here $H$ is the wave height from the crest to the trough in physical variables. The limiting Stokes wave emerges as the singularity reaches the fluid surface. Tables of Padé approximation for Stokes waves of different heights are provided. These tables allow to recover the Stokes wave with the relative accuracy of at least $10^{-26}$. The tables use from several poles for near-linear Stokes wave up to about hundred poles to highly nonlinear Stokes wave with $v_c/\lambda \sim 10^{-6}$.

**Key words:**

---

† Email address for correspondence: plushnik@math.unm.edu

## 1. Introduction

Theory of spatially periodic progressive (propagating with constant velocity without change of the shape and amplitude) waves in two-dimensional (2D) potential flow of an ideal incompressible fluid with free surface in gravitational field was founded in pioneering works by Stokes (1847, 1880*a*) and developed further by Michell (1893), Nekrasov (1921, 1951), and many others (see e.g. a book by Sretenskii (1976) for review of older works as well as Baker & Xie (2011); Cowley *et al.* (1999); Grant (1973); Longuet-Higgins (2008); Longuet-Higgins & Fox (1977, 1978); Schwartz (1974); Tanveer (1991); Williams (1981, 1985) and references there in for more recent progress). There are two major approaches to analyze the Stokes wave, both originally developed by Stokes. The first approach is the perturbation expansion in amplitude of Stokes wave called by the Stokes expansion. That approach is very effective for small amplitudes but converges very slowly (or does not converge at all, depending on the formulation according to Drennan *et al.* (1992)) as the wave approaches to the maximum height $H = H_{max}$ (also called by the Stokes wave of the greatest height or the limiting Stokes wave). Here the height $H$ is defined at the vertical distance from the crest to the trough of Stokes wave over a spatial period $\lambda$. The second approach is to consider the limiting Stokes wave, which is the progressive wave with the highest nonlinearity. Using conformal mappings Stokes found that the limiting Stokes wave has the sharp angle of $2\pi/3$ radians on the crest (Stokes 1880*b*), i.e. the surface is non-smooth (has a jump of slope) at that spatial point. That corner singularity explains a slow convergence of Stokes expansion as $H \to H_{max}$. The global existence of the limiting Stokes wave was proven by Toland (1978) however lacking a proof of a Stokes conjecture that the the jump of the slope at the crest is exactly $2\pi/3$ radians. The Stokes conjecture was later independently proven by Plotnikov (1982) and Amick *et al.* (1982).

It was Stokes (1880*b*) who first proposed to use conformal mapping in order to address finite amplitude progressive waves. In this paper we consider a particular case of potential flow of the ideal fluid of infinite depth although more general case of fluid of arbitrary depth can be studied in a similar way. Assume that free surface is located at $y = \eta(x,t)$, where $x$ is the horizontal coordinate, $y$ is the vertical coordinate, $t$ is the time and $\eta(x,t)$ is the surface elevation with respect to the zero mean level of fluid, i.e. $\int_{-\infty}^{\infty} \eta(x,t)\mathrm{d}x = 0$. We consider the conformal map between the domain $-\infty < y \leqslant \eta(x,t),\ -\infty < x < \infty$ of the complex plane $z \equiv x + \mathrm{i}y$ filled by the infinite depth fluid and a lower complex half-plane (from now on denoted by $\mathbb{C}^-$) of a variable $w \equiv u + \mathrm{i}v$ (see Fig. 1). The real line $v = 0$ is mapped into the free surface by $z(w)$ being the analytic function in the lower half-plane of $w$ as well as the complex fluid velocity potential $\Pi(w)$ is also analytic in $\mathbb{C}^-$. Both $z(w)$ and $\Pi(w)$ have singularities in upper half-plane (here and further denoted by $\mathbb{C}^+$).

The knowledge of singularities in $\mathbb{C}^+$ would result in the efficient description of the solution in the physical variables. Examples of such type of solutions in hydrodynamic-type systems are numerous including e.g. the dynamics of free surface of ideal fluid with infinite depth (Kuznetsov *et al.* 1993, 1994; Tanveer 1993) and finite depth (Dyachenko *et al.* 1996*b*), dynamics of interface between two ideal fluids (Kuznetsov *et al.* 1993), ideal fluid pushed through viscous fluid in a narrow gap between two parallel plates (Hele-Shaw flow) (Mineev-Weinstein *et al.* 2000), the dynamics of the interface between ideal fluid and light viscous fluid (Lushnikov 2004) and bubble pinch-off (Turitsyn *et al.* 2009). In these systems the dynamics is determined by poles/branch cuts in the complex plane. Related systems correspond to the spontaneous appearance of curvature singularities on vortex sheets as obtained by Moore (1979). Nie & Baker (1998) established that Moore's
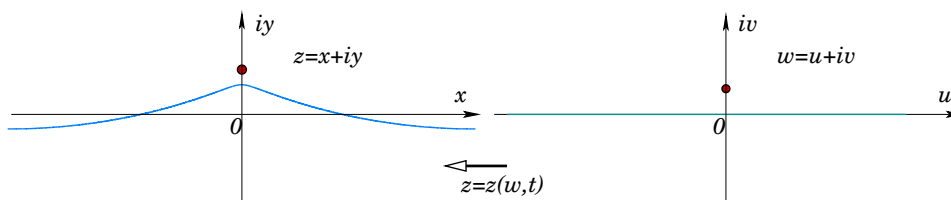
FIGURE 1. Schematic of a conformal map between the domain below the solid curve (left panel) in $z = x + iy$ complex plane and the lower complex half-plane in $w = u + iv$ (right panel). Fluid occupies the domain below the solid curve in physical plane $z = x + iy$. The solid curve of left panel (corresponds to a free surface of the fluid) is mapped into the real line (another solid line) in right panel. One spatial period of Stokes wave is shown by solid lines in both panels in the reference frame moving with the velocity $c$. The dark circles mark the positions of the singularity closest to the fluid surface in both panels.

singularities are present in axisymmetric vortex sheets. Inogamov & Oparin (2003) considered cone-shaped nose of $2\pi/3$ degrees in axisymmetric flow. Ishihara & Kaneda (1994) and Hou & Hu (2003) extended Moore's singularities to three-dimensional (3D) vortex sheets. Opposite limit is the global existence of water waves for small enough data shown both for 2D (Wu 2009) and 3D (Wu 2011) flows.

In this paper we determine that for Stokes wave the lowest singularities in $\mathbb{C}^+$ of both $z(w)$ and $\Pi(w)$ are the square-root branch points located periodically at $w = n\lambda + iv_c - ct$, $n = 0, \pm 1, \pm 2, ...$ (we choose the crests of Stokes wave to be located at $w = n\lambda - ct$) and we determine $v_c$ numerically as a function of $H/\lambda$. Here $c$ is the velocity of propagation of Stokes wave which depends on $H$. In the previous work Dyachenko *et al.* (2013) we found that as $H \to H_{max}$, the branch point approaches real axis with the scaling law

$$v_c \propto (H_{max} - H)^\delta, \tag{1.1}$$

where $\delta = 1.48 \pm 0.03$. We also provided an accurate estimation of maximum amplitude of the Stokes wave $H_{max}$. Adiabatically slow approach of Stokes wave to its limiting form during wave dynamics is one of the possible routes to wave breaking and whitecapping, which are responsible for significant part of energy dissipation for gravity waves (Zakharov *et al.* 2009, 2007). Formation of a close to limiting Stokes wave is also considered to be a probable final stage of evolution of a freak (or rogue) waves in the ocean resulting in formation of approximate limiting Stokes wave for a limited period of time with following wave breaking and disintegration of the wave or whitecapping and attenuation of the freak wave into wave of regular amplitude (Rainey & Longuet-Higgins 2006; Zakharov *et al.* 2006).

The paper is organized as follows. In Section 2 we introduce the basic equations of 2D hydrodynamics in conformal conformal variables and reduce these equations to the equation for Stokes wave. In Section 3 numerical approaches to simulation of Stokes wave are given together with the results of simulations. Also numerical procedures to recover the location and type of the branch point are discussed. Section 4 introduces a new variable $\zeta$ defining a second conformal transformation which maps one spatial period of Stokes wave into the entire real line. Then the Padé approximation of Stokes wave is found in complex $\zeta$ plane. The efficient Alpert-Greengard-Hagstrom (AGH) algorithm (Alpert *et al.* 2000; Lau 2004) is used to obtain the Padé approximation. That algorithm allows to avoid the appearance of artificial zeros and poles of Padé approximation and achieves a spectral accuracy. The convergence of the Padé approximation to the branch cut singularity is established which allows to recover the jump at branch cut. Section 5

relates jump at the branch cut in $\zeta$ variable to the sum of periodically located branch cuts in $w$ complex plane. It is shown how to use the series expansion of the jump along branch cuts near branch points to recover the square-root singularity at the branch point. It is demonstrated that there are no more singularities in the finite complex plane beyond one branch point $w = iv_c$ per period. In Section 6 the main results of the paper are discussed. Appendix A provides a derivation of basic hydrodynamic equations in conformal variables. Appendix B gives a short description of AGH algorithm adapted for Stokes wave. Appendix C describes a notation used for the tables of Padé approximants for Stokes wave and gives samples of such tables. A full set of tables is provided in the electronic attachment. These tables reproduce the Stokes wave with the relative accuracy of at least $10^{-26}$.

## 2. Basic equations

In physical coordinates $(x, y)$ a velocity $\mathbf{v}$ of $2D$ potential flow of inviscid incompressible fluid is determined by a velocity potential $\Phi(x, y, t)$ as $\mathbf{v} = \nabla\Phi$. The incompressibility condition $\nabla \cdot \mathbf{v} = 0$ results in the Laplace equation

$$\nabla^2 \Phi = 0 \tag{2.1}$$

inside fluid $-\infty < y < \eta(x, t)$. To obtain the closed set of equations we add the decaying boundary condition at large depth $\Phi(x, y, t)|_{y \to -\infty} = 0$, the kinematic boundary condition

$$\frac{\partial \eta}{\partial t} = \left( -\frac{\partial \eta}{\partial x}\frac{\partial \Phi}{\partial x} + \frac{\partial \Phi}{\partial y} \right)\bigg|_{y=\eta(x,t)} \tag{2.2}$$

and the dynamic boundary condition

$$\left( \frac{\partial \Phi}{\partial t} + \frac{1}{2}\left(\nabla\Phi\right)^2 \right)\bigg|_{y=\eta(x,t)} + g\eta = 0 \tag{2.3}$$

at the free surface

$$y = \eta(x, t). \tag{2.4}$$

We define the boundary value of the velocity potential as

$$\Phi(x, y, t)|_{y=\eta(x,t)} \equiv \psi(x, t), \tag{2.5}$$

Consider a time-dependent conformal transformation

$$z = z(w, t), \quad w = u + iv \tag{2.6}$$

which maps a half-strip $-\frac{\lambda}{2} \leqslant u < \frac{\lambda}{2}$, $-\infty < v \leqslant 0$ of complex plane $w$ into a region $-\frac{\lambda}{2} \leqslant x < \frac{\lambda}{2}$, $-\infty < y \leqslant \eta(x, t)$ of complex physical plane $z = x + iy$ at each time $t$ such that the line $-\frac{\lambda}{2} \leqslant u < \frac{\lambda}{2}$, $v = 0$ is mapped into a line of free surface $x + i\eta(x, t)$ with $-\frac{\lambda}{2} \leqslant x < \frac{\lambda}{2}$ and

$$x\left(-\frac{\lambda}{2}\right) = -\frac{\lambda}{2}, \quad x\left(\frac{\lambda}{2}\right) = \frac{\lambda}{2}. \tag{2.7}$$

Also $w = -i\infty$ maps into $z = -i\infty$. Here the flow is assumed to be periodic in the horizontal direction with the period $\lambda$ both in $w$ and $z$ variables. Conditions (2.7) suggest to separate $z(w, t)$ into a periodic part $\tilde{z}(w, t)$ and a non-periodic part $w$ as follows

$$z(w, t) = w + \tilde{z}(w, t), \text{ or } x(w, t) = u + \tilde{x}(w, t), \quad \tilde{y}(w, t) = v + y(w, t), \tag{2.8}$$

where

$$\tilde{z}(w + \lambda) = \tilde{z}(w), \quad \tilde{x}\left(\pm\frac{\lambda}{2}\right) = 0. \tag{2.9}$$

Equations (2.8) and (2.9) extend conformal transformation (2.6) into $\mathbb{C}^-$. Also $x(u,t)$ and $y(u,t)$ form a parametric representation (over the parameter $u$) of the free surface elevation (2.4).

The idea of using time-dependent conformal transformation for unsteady fluid flow was exploited by several authors including Ovsyannikov (1973), Meison *et al.* (1981), Tanveer (1991, 1993), and Dyachenko *et al.* (1996a); Zakharov *et al.* (2002b). We follow Dyachenko *et al.* (1996a) to recast the system (2.1)-(2.3) into the equivalent form for $x(u,t)$, $y(u,t)$ and $\psi(u,t)$ at the real line $w = u$ of the complex plane $w$ using the conformal transformation (2.6) (see Appendix A for more details). A kinematic boundary condition (2.2) is reduced to

$$y_t x_u - x_t y_u + \hat{H}\psi_u = 0 \tag{2.10}$$

and the dynamic boundary condition (2.3) is given by

$$\psi_t y_u - \psi_u y_t + g y y_u = -\hat{H}\left(\psi_t x_u - \psi_u x_t + g y x_u\right), \tag{2.11}$$

where

$$\hat{H}f(u) = \frac{1}{\pi}\text{p.v.}\int_{-\infty}^{+\infty}\frac{f(u')}{u' - u}\mathrm{d}u' \tag{2.12}$$

is the Hilbert transform with p.v. meaning a Cauchy principal value of integral. Periodicity of $f(u)$ allows to reduce the integration in the Hilbert transform as follows

$$\hat{H}f(u) = \frac{1}{\pi}\sum_{n=\infty}^{\infty}\text{p.v.}\int_{-\lambda/2}^{\lambda/2}\frac{f(u')}{u' - u + n\lambda}\mathrm{d}u' = \frac{1}{\lambda}\text{p.v.}\int_{-\lambda/2}^{\lambda/2}\frac{f(u')}{\tan\left(\pi\frac{u'-u}{\lambda}\right)}\mathrm{d}u'. \tag{2.13}$$

The equivalence of equations (2.10) and (2.11) to equations (2.1)-(2.3) uses the analyticity of $z(w)$ and $\Pi(w)$ in $\mathbb{C}^-$, where

$$\Pi = \Phi + \mathrm{i}\Theta \tag{2.14}$$

is the complex velocity potential. Here $\Theta$ is the stream function defined by $\Theta_x = -\Phi_y$ and $\Theta_y = \Phi_x$ to satisfy Cauchy-Riemann conditions for analyticity of $\Pi(z,t)$ in $z$ plane. The conformal transformation (2.6) ensures that

$$\Theta_u = -\Phi_v, \quad \Theta_v = \Phi_u \tag{2.15}$$

in $w$ plane. The periodicity of the flow implies the condition

$$\Pi(w + \lambda, t) = \Pi(w, t) \tag{2.16}$$

together with equation (2.9). We also assumed in equations (2.10) and (2.11) that

$$\int_{-\lambda/2}^{\lambda/2}\eta(x,t)\mathrm{d}x = \int_{-\lambda/2}^{\lambda/2}y(u,t)x_u(u,t)\mathrm{d}u = 0, \tag{2.17}$$

meaning that the elevation of free surface of unperturbed fluid is set to zero. The equation (2.17) is valid at all times and reflects a conservation of the total mass of fluid.

Both equations (2.10) and (2.11) are defined on the real line $w = u$. The Hilbert operator $\hat{H}$ transforms into the multiplication operator

$$(\hat{H}f)_k = \mathrm{i}\,\text{sign}\,(k)\,f_k, \tag{2.18}$$

for the Fourier coefficients (harmonics) $f_k$,

$$f_k = \frac{1}{\lambda} \int\limits_{-\lambda/2}^{\lambda/2} f(u) \exp\left(-\mathrm{i}ku\frac{2\pi}{\lambda}\right) \mathrm{d}u, \tag{2.19}$$

of the periodic function $f(u) = f(u + \lambda)$ represented through the Fourier series

$$f(u) = \sum_{k=-\infty}^{\infty} f_k \exp\left(\mathrm{i}ku\frac{2\pi}{\lambda}\right). \tag{2.20}$$

Here $\mathrm{sign}(k) = -1, 0, 1$ for $k < 0$, $k = 0$ and $k > 0$, respectively.

The Fourier series (2.20) allows to rewrite $f(u) = f(w)|_{v=0}$ as follows

$$f(u) = f^+(u) + f^-(u) + f_0, \tag{2.21}$$

where

$$f^+(w) = \sum_{k=1}^{\infty} f_k \exp\left(\mathrm{i}kw\frac{2\pi}{\lambda}\right) \tag{2.22}$$

is the analytical function in $\mathbb{C}^+$,

$$f^-(w) = \sum_{k=-\infty}^{-1} f_k \exp\left(\mathrm{i}kw\frac{2\pi}{\lambda}\right) \tag{2.23}$$

is the analytical function in $\mathbb{C}^-$ and $f_0 = const$ is the zero harmonic of Fourier series (2.20). In other words, equation (2.21) decompose $f(u)$ into the sum of functions $f^+(u)$ and $f^-(u)$ which are analytically continued from the real line $w = u$ into $\mathbb{C}^+$ and $\mathbb{C}^-$, respectively. Equations (2.18), (2.21), (2.22) and (2.23) imply that

$$\hat{H}f(u) = \mathrm{i}\left[f^+(u) - f^-(u)\right]. \tag{2.24}$$

If function $f(w)$ is analytic in $\mathbb{C}^-$ then $\bar{f}(\bar{w})$ is analytic in $\mathbb{C}^+$ as follows from equations (2.21)-(2.23), where bar mean complex conjugation, $\bar{w} = u - \mathrm{i}v$. Then the function $\bar{f}(u)$, $u \in \mathbb{R}$ has analytic continuation into $\mathbb{C}^+$ because at the real line $w = \bar{w}$. Using equations (2.5) and (2.14) we obtain that $\psi(u,t) = \frac{1}{2}[\Pi(u,t) + \bar{\Pi}(u,t)]$. It means that after solving equations (2.10) and (2.11) one can recover the complex potential $\Pi$ from the analytical continuation of

$$\Pi(u,t) = 2\hat{P}\psi(u,t) \tag{2.25}$$

into $\mathbb{C}^-$. Here

$$\hat{P} = \frac{1}{2}(1 + \mathrm{i}\hat{H}) \tag{2.26}$$

is the projector operator, $\hat{P}f = f^- + \frac{f_0}{2}$, into a function which has analytical continuation from the real line $w = u$ into $\mathbb{C}^-$, as follows from equation (2.24). Note that without loss of generality we assumed the vanishing zero Fourier harmonic, $\Pi_0 = 0$, for $\Pi(u,t)$.

Also

$$\hat{H}^2 f = -f \tag{2.27}$$

for the function $f(u)$ defined by (2.21) provided the additional restriction that $f_0 = 0$ holds. In other words, the Hilbert transformation is invertible on the class of functions represented by their Fourier series provided zeroth Fourier harmonic $f_0$ vanishes. If $f_0 \neq 0$ then the identity (2.27) is replaced by

$$\hat{H}^2 f = -(f - f_0). \tag{2.28}$$

The analyticity of $z(w)$ in $\mathbb{C}^-$ implies, together with $\tilde{x} = \frac{1}{2}(\tilde{z} + \bar{\tilde{z}})$, $\tilde{y} = \frac{1}{2i}(\tilde{z} - \bar{\tilde{z}})$ and equations (2.24),(2.28), that at the real line $w = u$ the following relations hold

$$y - \tilde{y}_0 = \hat{H}\tilde{x} \quad \text{and} \quad \tilde{x} - \tilde{x}_0 = -\hat{H}y. \tag{2.29}$$

Here $\tilde{x}_0$ and $\tilde{y}_0$ are zero Fourier harmonics of $\tilde{x}(u,t)$ and $y(u,t)$, respectively. Note that the addition of zero harmonics $\tilde{x}_0$ and $\tilde{y}_0$ into equation (2.29) is the modification compare with Refs. Dyachenko *et al.* (1996*a*); Zakharov *et al.* (2002*a*). These Refs. were focused on the decaying boundary conditions $\eta(x,t) \to 0$ and $\psi(x,t) \to 0$ for $|x| \to \infty$ which imply, together with the condition (2.17) in the limit $\lambda \to \infty$, that $\tilde{x}_0 = \tilde{y}_0 = 0$. However, generally $\tilde{x}_0$ and $\tilde{y}_0$ might be nonzero for the periodic solutions with a finite $\lambda$ considered in this paper.

Equations (2.29) imply that it is enough to find either $y(u,t)$ or $x(u,t)$ then the second of them is recovered by these explicit expressions. Taking derivative of equations (2.29) with respect to $u$ results in the similar relations

$$y_u = \hat{H}\tilde{x}_u \quad \text{and} \quad \tilde{x}_u = -\hat{H}y_u, \tag{2.30}$$

### 2.1. *Progressive waves*

Stokes wave corresponds to a solution of the system (2.10) and (2.11) in the traveling wave form

$$\psi(u,t) = \psi(u - ct), \ \tilde{z}(u,t) = \tilde{z}(u - ct), \tag{2.31}$$

where both $\psi$ and $\tilde{z}$ are the periodic functions of $u - ct$. Here $c$ is the phase velocity of Stokes wave. We transform into the moving frame of reference, $u - ct \to u$, and assume that the crest of the Stokes wave is located at $u = 0$ as in Fig. 1 and $\lambda$ is the spatial period in $u$ variable for both $\psi$ and $\tilde{z}$ in equation (2.31). We look for the Stokes wave which has one crest per period. Higher order progressive waves are also possible which have more than one different peak per period Chen & Saffman (1980). However here we consider only Stokes wave. We recall that the spatial period $\lambda$ is the same in both $u$ and $x$ variables as follows from equation (2.9). In addition, it implies that the phase velocity is the same both in $u$ and $x$ variables so that the Stokes wave has the moving surface $y = \eta(x - ct)$ and the velocity potential $\psi = \psi(x - ct)$ in physical spatial variables $(x, y)$ with the same value of $c$ as in equations (2.31). The Stokes solution requires $y(u)$ to be the even function while $\tilde{x}(u)$ needs to be the odd function which ensures that $y = \eta(x - ct)$ is the even function.

It follows from (2.10) and (2.31) (corresponding to substitution $\frac{\partial}{\partial t} \to -c\frac{\partial}{\partial u}$ for $y$ and $\psi$ and $\frac{\partial x}{\partial t} \to -c\frac{\partial \tilde{x}}{\partial u}$) that $\hat{H}\psi_u = cy_u$ and then excluding $\psi$ from (2.11) we obtain that

$$-c^2 y_u + gyy_u + g\hat{H}[y(1 + \tilde{x}_u)] = 0. \tag{2.32}$$

We now apply $\hat{H}$ to (2.32), use (2.29) to obtain a closed expression for $y$, and introduce the operator $\hat{k} \equiv -\partial_u \hat{H} = \sqrt{-\nabla^2}$ which results in the following expression

$$\hat{L}_0 y \equiv \left(c^2\hat{k} - 1\right)y - \left(\frac{\hat{k}y^2}{2} + y\hat{k}y\right) = 0, \tag{2.33}$$

where we made all quantities dimensionless by the following scaling transform $u \to u\lambda/2\pi$, $x \to x\lambda/2\pi$, $y \to y\lambda/2\pi$ and $c$ is scaled by $c_0$ as follows $c \to c\,c_0$, where $c_0 = \sqrt{g/k_0}$ is the phase speed of linear gravity wave with the wavenumber $k_0 = 2\pi/\lambda$. In these scaled units the period of $\psi$ and $\tilde{z}$ is $2\pi$. Our new operator $\hat{k}$ in Fourier space acts as multiplication operator, qualitatively similar to $\hat{H}$: $(\hat{k}f)_k = kf_k$.

## 3. Numerical simulation of Stokes wave

We solve (2.33) numerically to find $y(u)$ by two different methods each of them beneficial for different range of the parameter $H/\lambda$. For both methods $y(u)$ was expanded in cosine Fourier series and the operator $\hat{k}$ was evaluated numerically using Fast Fourier Transform (FFT). A uniform grid with $M$ points was used for the discretization of $-\pi \leqslant u < \pi$. A first method is inspired by a Petviashvili method (Petviashvili 1976) which was originally proposed to find solitons in nonlinear Schrödinger (NLS) equation as well as it was adapted for nonlocal NLS-type equations, see e.g. Lushnikov (2001). We used a version generalized Petviashvili method (GPM) (Lakoba & Yang 2007; Pelinovsky & Stepanyants 2004) adjusted to Stokes wave as described in Dyachenko *et al.* (2013). In practice this method allowed to find high precision solutions up to $H/\lambda \lesssim 0.1388$. The performance of that method for larger values of $H/\lambda$ was limited by the decrease of the speed of numerical convergence.

### 3.1. *Newton CG and Newton CR methods*

For larger $H/\lambda$ we used a second method which is the Newton Conjugate Gradient (Newton-CG) method proposed by Yang (2009, 2010). The idea behind the Newton-CG method is simple and aesthetic: first, linearize (2.33) about the current approximation $y_n$, assuming that the exact solution can be written as a sum of current approximation and a correction $y = y_n + \delta y_n$: $\hat{L}_0 y = 0$. Then $\hat{L}_0 y_n + \hat{L}_1 \delta y_n \simeq 0$, where $\hat{L}_1 = -\hat{M}\delta y_n - \left(\hat{k}(y_n \delta y_n) + y_n \hat{k}\delta y_n + \delta y_n \hat{k} y_n\right)$ is the linearization of $\hat{L}_0$ around the current approximation $y_n$ and $\hat{M} \equiv -c^2\hat{k} + 1$. Second, solve the resulting linear system $\hat{L}_1 \delta y_n = -\hat{L}_0 y_n$ for $\delta y_n$ with one of standard numerical methods, in our case it was either Conjugate Gradient (CG) method (Hestenes & Stiefel 1952) or Conjugate Residual (CR) method (Luenberger 1970) to obtain next approximation $y_{n+1} = y_n + \delta y$. It should be noted that monotonic convergence of CG or CR methods is proven only for positive definite (semidefinite for CR) operators, while in our case $\hat{L}_1$ is indefinite. Nevertheless, both methods were converging (although generally nonmonotonically) to the solutions, and convergence was much faster than using GPM.

Newton-CG/CR methods can be written in either Fourier space, or in physical space. We considered both cases, however Newton-CG/CR methods in Fourier space require four fast Fourier transforms per CG/CR step, while in physical space it requires at least six. For both cases CG and CR we used $\hat{M}$ as a preconditioner.

We found that the region of convergence of the Newton-CG/CR methods to nontrivial physical solution (2.33) is relatively (with respect to GPM) narrow and requires an initial guess $y_0$ to be quite close to the exact solution $y$. In practice we first run GPM and then choose $y_0$ for Newton-CG/CR methods as the last available iterate of GPM.

Because most of our interest was in getting dependence of characteristics of Stokes waves on the wave height and the only parameter in equation (2.33) is velocity of propagation $c$, we were calculating waves changing continuously the parameter $c$ and using results of computations with previous values of $c$ as initial condition $y_0$ for the Newton CG/CR iterations. Due to this approach Newton-CG/CR methods converge to the nontrivial solution in all cases provided we additionally used the numerical procedure described below in Section 3.2.

### 3.2. *Stokes wave velocity as a function of steepness*

Results of multiple simulations of Stokes wave are shown in Figure 2, where the wave velocity $c$ is shown as a function of the dimensionless wave height $H/\lambda$. This function is nonmonotonic which is in agreement with previous simulations (e.g. Schwartz (1974);
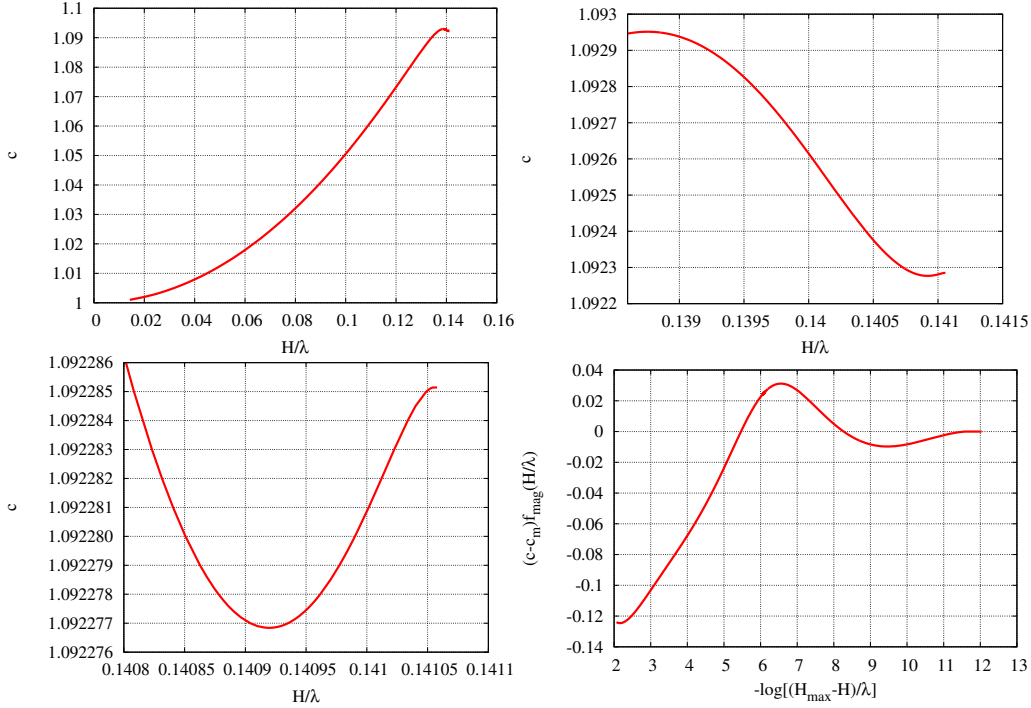
FIGURE 2. Oscillations of dimensionless velocity of Stokes wave propagation as function of steepness obtained from simulations. First three plots from left to right and from top to bottom have increasing zoom both in vertical and horizontal axes to focus on oscillations. In the lower right corner a plot is scaled by a magnification function $f_{mag}(H/\lambda) = 1/(30(H_{max}-H)/\lambda)^{1.15}+1$ to show all simulation data in a single graph while stressing obtained oscillations.

Williams (1981, 1985)) and theoretical analysis (Longuet-Higgins & Fox (1977, 1978)) which predicted an infinite number of oscillations.

We were able to resolve with quadruple precision two oscillations (two maxima and two minima) of the propagation velocity as a function of $H/\lambda$. These oscillations represent a challenge for simulation, because propagation velocity is the only parameter in the equation (2.33). Then it is impossible even to go over the first maximum by changing continuously velocity of propagation $c$. This is because after the maximum is reached, we has to start decreasing the parameter $c$. But decreasing of $c$ causes iterations to converge to the less steep solution on the left from the maximum (which we already obtained on previous steps), instead of steeper solutions to the right from the maximum.

In order to resolve this issue we used the following approach. Assume that the singularity of $\tilde{z}$ closest to real axis in $w$ complex plane is the branch point

$$\tilde{z} \simeq c_1(w - \mathrm{i}v_c)^\beta \tag{3.1}$$

for $w \to \mathrm{i}v_c$, where $c_1$ is the complex constant, $v_c > 0$ and $\beta$ are real constants. By the periodicity in $u$, similar branch points are located at $w = \mathrm{i}v_c + 2\pi n$, $n = \pm 1, \pm 2, \ldots$ (recall that that we already switched to the dimensionless coordinates). We expand $\tilde{z}(u)$
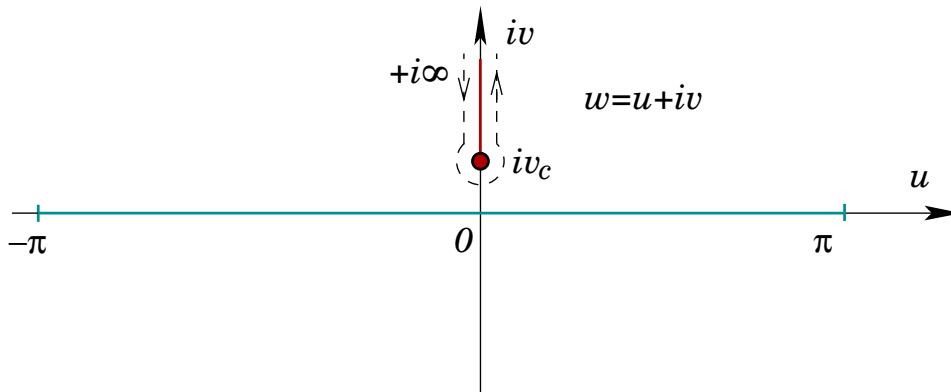
FIGURE 3. Schematic of contour in the $\mathbb{C}^+$ which allows to determine distance $v_c$ from the branch cut to the real axis.

into Fourier series $\tilde{z}(u) = \sum\limits_{-\infty}^{k=0} \hat{\tilde{z}}_k \exp(iku)$, where

$$\hat{\tilde{z}}_k = \frac{1}{2\pi} \int\limits_{-\pi}^{\pi} \tilde{z}(u) e^{-iku} du \tag{3.2}$$

are Fourier coefficients and the sum is taken over nonpositive integer values of $k$ which ensures both $2\pi$-periodicity of $\tilde{z}(u)$ and analyticity of $\tilde{z}(w)$ in $\mathbb{C}^-$. We evaluate (3.2) in the limit $k \to -\infty$ by moving the integration contour from the line $-\pi < u < \pi$ into $\mathbb{C}^+$ until it hits the lowest branch point (3.1) so it goes around branch point and continues straight upwards about both sides of the corresponding branch cut as shown by the dashed line in right panel of Fig. 3. Here we assume that branch cut is a straight line connecting $w = iv_c$ and $+i\infty$. Then the asymptotic of $|\hat{\tilde{z}}_k|$ is given by

$$|\hat{\tilde{z}}_k| \propto |k|^{-1-\beta} e^{-|k|v_c}, \quad k \to -\infty. \tag{3.3}$$

This approach was used in our previous work (Dyachenko *et al.* 2013) to evaluate distance $v_c$ of the lowest singularity to the real line. Now our key idea is to push artificially the singularity $w = iv_c$ toward the real line, thus increasing $H/\lambda$. It follows from expression (3.3) that to decrease $v_c$ we can multiply Fourier coefficients of the previously obtained Stokes wave solution $\hat{\tilde{z}}_k$ by $\exp(\alpha k)$, where the numerical parameter $\alpha$ is chosen such that $0 < \alpha \ll v_c$. The result of this multiplication $\hat{\tilde{z}}_k \exp(\alpha k)$ is not a Stokes wave solution anymore, but it has higher steepness and not very distinct from the Stokes wave solution if $\alpha$ is small enough. After that modification we slightly decrease $c$ from previous value and allow iterations of Section 3.1 to converge starting from $\hat{\tilde{z}}_k \exp(\alpha k)$ as zero iteration. As we expected, iterations then converge to the solution on the right from the maximum. This procedure allowed us to resolve both maxima and one nontrivial minimum of $c$ as a function of $H/\lambda$ as summarized in Fig. 2.

### 3.3. Recovering $v_c$ from the Fourier spectrum of Stokes wave

To obtain the location of the branch point $w = iv_c$ with good precision one has to go beyond the leading order asymptotic (3.3). Next order corrections to the integral (3.2) for $\beta = 1/2$ have the following form

$$|\hat{\tilde{z}}_k| \simeq \left( c_1 |k|^{-3/2} + c_2 |k|^{-5/2} + c_3 |k|^{-7/2} + c_4 |k|^{-9/2} + \dots \right) e^{-|k|v_c}, \quad k \to -\infty, \tag{3.4}$$
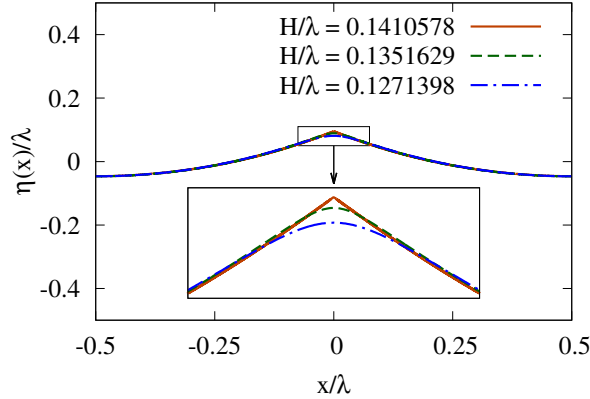
FIGURE 4. Stokes wave with $c = 1.082$ (blue dash-dotted line), $c = 1.091$ (green dashed line) and $c = 1.0922851405$ (dark orange solid line). Corresponding values of $H/\lambda$ are given in the legend. Inset shows zoom-in into small values of $x/\lambda$ near a wave crest.

where we took into account the expansion of $\tilde{z}(w)$ in half-integer powers $(w - \mathrm{i}v_c)^{1/2+n}$, $n = 0, 1, 2, \ldots$ beyond the leading order term (3.1).

The numerically obtained spectrum $|\hat{\tilde{z}}_k|$ of Stokes wave was fitted to the expansion (3.4) in order to recover $v_c$ and coefficients $c_1$, $c_2$, $c_3$, …. The highest accuracy in recovering $v_c$ was achieved when the middle of spectrum $k \sim k_{max}/2$ was used for that fit, there $k_{max} = M/2$ is the highest Fourier harmonic used in simulations. $k_{max}/2$ represent a compromise between the highest desired values of $k$ to be as close as possible to asymptotic regime $k \to \infty$ and the loss of numerical precision for $k \to k_{max}$. We estimated the accuracy of the fit by varying values of $k$ used for fitting as well as changing the number of terms in the expansion (3.4). Typically we used 4 terms in (3.4). Section 4.3 discusses the comparison of the accuracy of the obtained results with the other methods we used to find $v_c$.

### 3.4. *Highest wave obtained*

We calculated $\tilde{z}(u)$ with high accuracy for different values of $H/\lambda$ using computations in quad precision (32 digits). Such high precision is necessary to reveal the structure of singularities in $\mathbb{C}^+$. Fig. 4 shows spatial profiles of Stokes waves for several values of $H/\lambda$ in physical variables $(x, y)$. The Stokes wave quickly approaches the profile of limiting wave except a small neighborhood of the crest.

As it was shown in the previous paper Dyachenko *et al.* (2013), tails of the spectra have asymptotic behavior corresponding to $\beta = 1/2$ in (3.3), which means that we have square root branch cut singularity in $\mathbb{C}^+$ all the time. This is consistent with theoretical predictions by Grant (1973) and Tanveer (1991).

The number of Fourier modes $M \equiv 2k_{max}$ which we used in Fast Fourier Transform (in simulations we expand $y(u)$ in cosine Fourier series to speed up simulations and to be memory efficient) for each value $H/\lambda$ increases quickly with the increase of $H$ as $v_c$ decreases. E.g., for $H/\lambda = 0.0994457$ it was more than enough to use 256 modes while for the largest wave height

$$H_{max}^{num}/\lambda = 0.14105777885488320816492860 2256956 \tag{3.5}$$

achieved in simulations we used $M = 2^{27} \approx 134 \times 10^6$ modes. Due to such high number of modes, the precision of value (3.5) decreases by round-off errors in approxi-

mately $M^{1/2}$ times, i.e. in $\sim 4$ digits. This extreme case has $c = 1.0922851405$ and $v_c = 5.93824419892803271779 \times 10^{-7}$. These numbers are the moderate extension of our previous work Dyachenko *et al.* (2013) by pushing down a lowest value of $v_c$ more than twice. Further decrease of the numerical values of $v_c$ can be achieved by both subtracting the leading order singularity (3.1) from the numerical solution and using the nonuniform numerical grid in $u$ which concentrates near $u = 0$. These numerical approaches are however beyond the scope of this papers.

Before our work Dyachenko *et al.* (2013), the numerical estimates of $H_{max}$ were found by Williams (1985) as $H_{max}^{Williams}/\lambda = 0.141063$ and Gandzha & Lukomsky (2007) $H_{max}^{GL}/\lambda = 0.14106348398$. The other commonly used but less precise estimate is $H_{max}^{Schwartz}/\lambda = 0.1412$ (Schwartz 1974). It was shown in Dyachenko *et al.* (2013) that numerical values of $v_c$ in the limit $(H_{max} - H)/\lambda \ll 0$ was fitted to the scaling law (1.1) with

$$H_{max}/\lambda = 0.1410633 \pm 4 \cdot 10^{-7}. \tag{3.6}$$

The mean-square error for $\delta$ in (1.1) is $\simeq 0.04$ which offers the exact value $\delta = 3/2$ as a probable candidate for (1.1). The estimate (3.6) suggests that the previous estimate $H_{max}^{Williams}$ is more accurate than $H_{max}^{Schwartz}$. Also $H_{max}^{GL}$ is within the accuracy of the estimate (3.6). However, $H_{max}^{GL}$ is obtained in Ref. Gandzha & Lukomsky (2007) from the Michell's expansion (Michell 1893) of the limiting Stokes wave which ignores the expansion in powers of the irrational number $\mu = 1.46934574\ldots$ Existence of that expansion beyond the Stokes power law $u^{2/3}$ was established by Grant (1973). Lack of resolving that expansion suggests that $H_{max}^{GL}$ does not have a well controlled accuracy. In contrast, our numerical results are based on Fourier series for non-limiting Stokes wave which has well-controlled precision. The difference between (3.6) and the new lower boundary estimate (3.5) of the largest $H$ is $\simeq 0.004\%$.

## 4. Padé approximation of Stokes wave

### 4.1. *Additional conformal transformation and spectral convergence of Padé approximation*

To analyze the structure of singularities of Stokes wave we perform an additional conformal transformation between the complex plane $w = u + iv$ and the complex plane for the new variable

$$\zeta = \tan\left(\frac{w}{2}\right). \tag{4.1}$$

Equation (4.1) maps the strip $-\pi < Re(w) < \pi$ into the complex $\zeta$ plane. In particular, the line segment $-\pi < w < \pi$ of the real line $w = u$ maps into the real line $(-\infty, \infty)$ in the complex plane $\zeta$ as shown in Fig. 5. Vertical half-lines $w = \pm\pi + iv$, $0 < v < \infty$ are mapped into a branch cut $i < \zeta < i\infty$. In a similar way, vertical half-lines $w = \pm\pi + iv$, $-\infty < v < 0$ are mapped into a branch cut $-i\infty < \zeta < i$. However, $2\pi$−periodicity of $\tilde{z}(w)$ (2.9) allows to ignore these two branch cuts because $\tilde{z}(w)$ is continuous across them. Complex infinities $w = \pm i\infty$ are mapped into $\zeta = \pm i$. An unbounded interval $[iv_c, i\infty)$, $v_c > 0$ is mapped into a finite interval $[i\chi_c, i)$ with

$$\chi_c = \tanh\frac{v_c}{2}. \tag{4.2}$$

The mapping (4.1) is different from the commonly used (see e.g. Schwartz (1974); Tanveer (1991); Williams (1981)) mapping $\zeta = \exp(-iw)$ (maps the strip $-\pi \leqslant Re(w) < \pi$ into the unit circle). The advantage of using the mapping (4.1) is the compactness of the
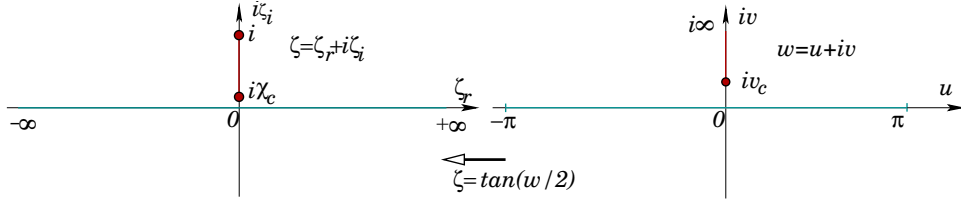
FIGURE 5. Schematic of a second conformal map between the periodic domain in $w$-plane (right panel) into $\zeta = \tan(w/2)$-plane. Another useful property of this map is representation of $2\pi$-periodic branch cut from $iv_c$ to $i\infty$ as a finite length cut from $\chi_c = \tan(iv_c/2)$ to i.
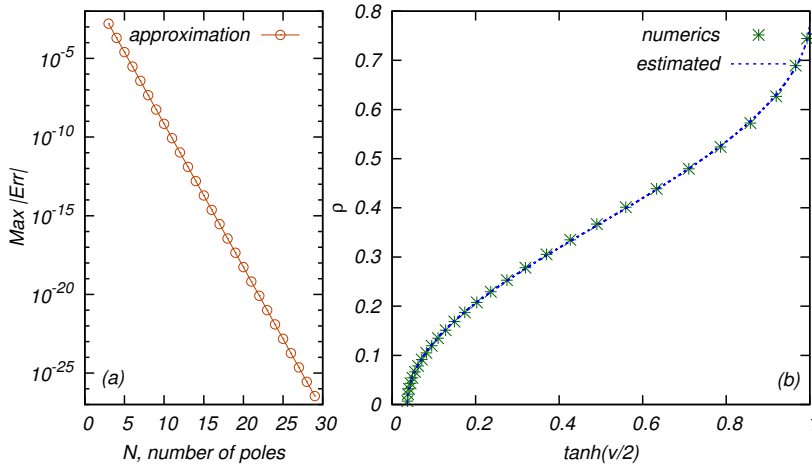


FIGURE 6. (a) An exponential decay of error in Padé approximation of Stokes for $H/\lambda = 0.12551024766621203351189812590805 3$ as a function of the number of poles $N$. (b) The density $\rho(\chi)$ on the branch cut sampled at $\zeta_k = i\chi_k \equiv i\tanh\left(\frac{v_k}{2}\right)$, $k = 1,,\ldots,N$, obtained from the Padé approximation of Stokes wave from(a) with $N = 29$ (green stars). Blue dotted line is the estimated profile of $\rho(\chi)$ for the same Stokes wave in the continuous limit of $N \to \infty$.

interval $(i\chi_c, i)$ as mapped from the infinite interval $(iv_c, i\infty)$. In contrast, the mapping to the circle leaves the interval $(iv_c, i\infty)$ infinite in $\zeta$ plane.

We use Alpert-Greengard-Hagstrom (AGH) algorithm (Alpert *et al.* 2000; Lau 2004) to approximate the Stokes wave $\tilde{z}(\zeta)$ at the real line $\mathrm{Re}(\zeta) = \zeta$ by a set a poles in the complex $\zeta$ plane. Approximation by a set of poles is a particular case of Padé approximation by rational functions $\frac{P(\zeta)}{Q(\zeta)}$, where $P(\zeta)$ and $Q(\zeta)$ are polynomials. Zeros of $Q(\zeta)$ give the location of poles. Looking at complex values of $\zeta$ in the rational function $\frac{P(\zeta)}{Q(\zeta)}$ provides the analytical continuation of $\tilde{z}(\zeta)$ into the complex $\zeta$ plane. Usually Padé approximation is numerically unstable because of the pairs of spurious zeros and poles appear in finite precision arithmetics. These doublets correspond to positions of zeros of $P(\zeta)$ and $Q(\zeta)$ which are nearly cancel each other. In our practical realizations, AGH algorithm avoids the numerical instability of the Padé approximation until the number of poles $N$ increases to reach the accuracy corresponding to the round-off error in the numerical approximation of $\tilde{z}(u)$. If the analytical continuation of $\tilde{z}(u)$ into $w \in \mathbb{C}$ has a branch cut, the AGH algorithm places poles along the branch cut. AGH algorithm is outlined in Appendix B.

We applied AGH algorithm for $\tilde{z}(\zeta)$ at the real line $\mathrm{Re}(\zeta) = \zeta$, where $\tilde{z}(\zeta)$ is obtained from simulations described in Section 3. Increasing $N$ we observed the exponential con-
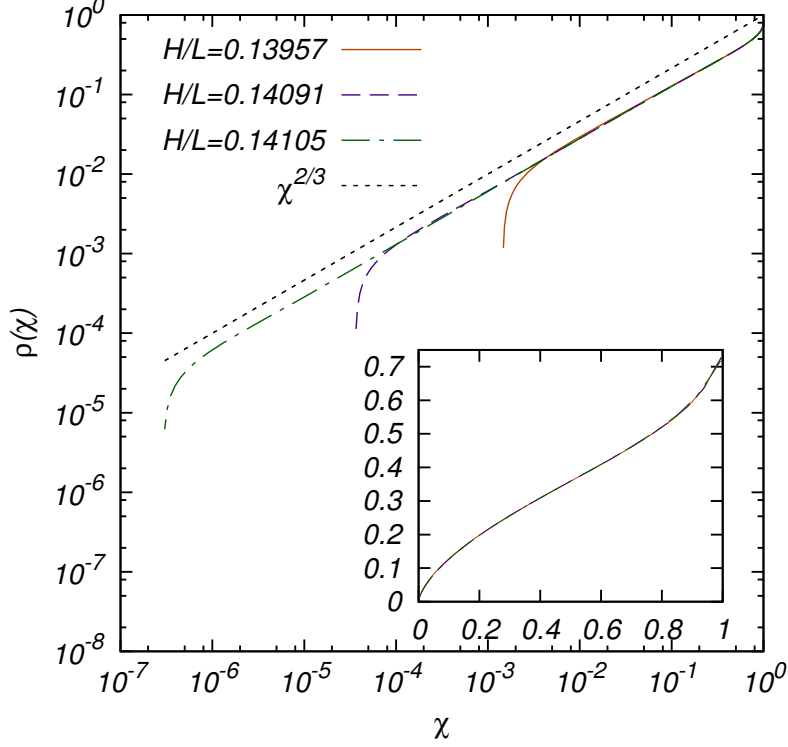
FIGURE 7. The density $\rho(\chi)$ for three different Stokes waves in log-log scale. A straight dashed line shows $\chi^{2/3}$ scaling law which corresponds to the limiting Stokes wave. Insert shows $\rho(\chi)$ in linear scale for the same three Stokes wave which are visually almost indistinguishable.

vergence of Padé approximation $z(\zeta)_{pade}$ to $\tilde{z}(\zeta)$ as

$$err_{\infty} \propto e^{-p(v_c)N}, \tag{4.3}$$

where $err_{\infty} \equiv \max\limits_{-\infty<\zeta<\infty} |\tilde{z}(\zeta) - \tilde{z}(\zeta)_{pade}|$ is the error in infinity (maximum) norm. An example of the exponential convergence is shown in Figure 6a for a particular Stokes wave. Here $p(v_c)$ is the function of $v_c$ but is independent on $N$. We found that with high precision

$$p(v_c) \propto v_c^{1/6}. \tag{4.4}$$

AGH algorithm is looking for poles in the entire complex plane $\zeta$. All the encountered poles for Stokes wave were found on the interval of imaginary axis along the interval $[i\chi_c, i)$, where $\chi_c$ is determined numerically as in Section 3.

Equations (4.3) and (4.4) demonstrate excellent performance of Padé approximation. E.g., decreasing $v_c$ by six order required in our simulations only 10-fold increase of $N$ as detailed in Appendix C. It suggests that numerical method which solves Stokes wave equation (2.33) directly in terms of Padé approximants might be superior to Fourier methods including numerical approaches mentioned in Section 3.3. This topic is however beyond the scope of this paper.

It is rather straightforward to distinguish in AGH algorithm poles from branch cuts. If both poles and branch cuts would be present in $\tilde{z}(\zeta)$ then increasing $N$ one observes that some poles of Padé approximation are not moving and their complex residues remain approximately the same. These correspond to poles of $\tilde{z}(\zeta)$. Such behavior occurs for

test problems when we artificially added extra poles to $\tilde{z}(\zeta)$. Other poles of Padé approximation are moving with the increase of $N$ and their complex residues are changing. These poles mark the spatial location of branch cuts of $\tilde{z}(\zeta)$. The density of poles along each branch cut is increasing with the increase of $N$. If the jump of $\tilde{z}(\zeta)$ at branch cut is continuous along it then we expect to see the convergence of density of poles with the increase of $N$. All this is valid until $err_\infty$ decreases down to the level of round-off error at which $\tilde{z}(\zeta)$ was determined. Further increase of $N$ would result in the appearance of spurious poles at random positions of $\zeta$ plane with the magnitudes of complex residues at the level of round off error ($\sim 10^{-32}$ for $z(\zeta)$ found with quad precision in Section 3).

Using $\tilde{z}(\zeta)$ obtained by the method of Section 3, we found a single branch cut $[i\chi_c, i)$ but no poles in Stokes wave. It means that in complex $w$ plane we have one branch cut per spatial period $2\pi$ located at $(2\pi n + iv_c, 2\pi n + i\infty)$, $n \in \mathbb{N}$.

We parametrize that branch cut as follows

$$\tilde{z}(\zeta) = iy_0 + \int_{\chi_c}^{1} \frac{\rho(\chi')d\chi'}{\zeta - i\chi'}, \tag{4.5}$$

where $\rho(\chi)$ is the density along branch cut. That density is related to the jump of $\tilde{z}(\zeta)$ at branch cut as explained in Section 5.1. The constant $y_0$ is determined by the value of $\tilde{z}(\zeta)|_{\zeta=\infty} = \tilde{z}(w)|_{w=\pi}$. This constant has a zero imaginary part, $\mathrm{Im}(y_0) = 0$, because $\tilde{x}(w)|_{w=\pi/2} = 0$ as given by the equation (2.9).

The Padé approximation represents equation (4.5) as follows

$$\tilde{z}(\zeta) = iy_0 + \int_{\chi_c}^{1} \frac{\rho(\chi')d\chi'}{\zeta - i\chi'} \simeq iy_0 + \sum_{n=1}^{N} \frac{\gamma_n}{\zeta - i\chi_n}, \tag{4.6}$$

where the numerical values of the pole positions $\chi_n$ and the complex residues $\gamma_n$ ($n = 1, \ldots, N$) are obtained from AGH algorithm.

### 4.2. *Recovering jump along branch cut*

We recover $\rho(\chi)$ from equation (4.6) as follows. Assume that we approximate the integral in equation (4.5) by the trapezoidal rule

$$\int_{\chi_c}^{1} \frac{\rho(\chi')d\chi'}{\zeta - i\chi'} \simeq \frac{\chi_2 - \chi_1}{2} \frac{\rho_1}{\zeta - i\chi_1}$$

$$+ \sum_{n=2}^{N-1} \frac{\chi_{n+1} - \chi_{n-1}}{2} \frac{\rho_n}{\zeta - i\chi_n} + \frac{\chi_N - \chi_{N-1}}{2} \frac{\rho_N}{\zeta - i\chi_N}. \tag{4.7}$$

A comparison of equations (4.6) and (4.7) suggests the approximation $\rho_{n,N}$ of the density $\rho(\chi_n)$ on the discrete grid $\chi_n$, $n = 1, \ldots, N$ as follows

$$\rho(\chi_n) \simeq \rho_{n,N} = \frac{2\gamma_n}{\chi_{n+1} - \chi_{n-1}} \quad \text{for } n = 2, \ldots, N-1, \tag{4.8a}$$

$$\rho(\chi_1) \simeq \rho_{1,N} = \frac{2\gamma_1}{\chi_2 - \chi_1}; \quad \rho(\chi_N) \simeq \rho_{N,N} = \frac{2\gamma_N}{\chi_N - \chi_{N-1}}. \tag{4.8b}$$

A convergence of $\rho_{n,N}$ to the continuous limit $\rho(\chi_n)$ as $N$ increases is quadratic with the error scaling $\propto \frac{1}{N^2}$ for $\chi$ away from boundaries $\chi = \chi_c$ and $\chi = 1$. Near these boundaries we cannot apply the trapezoidal rule and have to resort to less accurate

estimates given by the equation (4.8$b$). Figure 8 demonstrates this $\propto \frac{1}{N^2}$ convergence of the Pade approximation to the continuous limit. Figure 6b shows the particular example of $\rho(\chi)$ (shown by solid line solid line) compared with $\rho_{n,N}$ (shown by stars) for $N = 29$. We believe that the convergence of $\rho_n$ to the continuous value $\rho(\chi)$ as $N \rightarrow \infty$ and absence of other poles outside of $[i\chi_c, i]$ provide a numerical proof that the only singularity of $\tilde{z}(\zeta)$ are the branch points $i\chi_c$ and $i$ connected by the branch cut $\zeta \in [i\chi_c, i]$.

At $\chi = \chi_c$ the function $\rho(\chi)$ has a square root singularity as given below by equation (4.13). This singularity additionally reduces the accuracy of the approximation (4.8$b$) for $\rho_{1,N}$ which is based on Taylor series. To significantly improve numerical accuracy of $\rho_{1,N}$ we assume that $\rho$ has the following square root dependence in the vicinity of $\chi_c$:

$$\rho_{approx}(\chi) = A\sqrt{\chi - \chi_c}. \tag{4.9}$$

Here the values of the parameters $A$ and $\chi_c$ are determined from two interior points $(\chi_2, \rho_{2,N})$ and $(\chi_3, \rho_{3,N})$ found via the trapezoid rule (4.8$a$). We assume that $\rho_{approx}(\chi_2) = \rho_{2,N}$ and $\rho_{approx}(\chi_3) = \rho_{3,N}$ which gives that

$$A = \left( \frac{\rho_{3,N}^2 - \rho_{2,N}^2}{\chi_3 - \chi_2} \right)^{1/2}, \qquad \chi_c = \frac{\rho_{3,N}^2 \chi_2 - \rho_{2,N}^2 \chi_3}{\rho_{3,N}^2 - \rho_{2,N}^2}. \tag{4.10}$$

Using equations (4.9) and (4.10) for $\chi = \chi_1$ we obtain the numerically accurate approximation that

$$\rho_{1,N} = \left( \frac{(\chi_3 - \chi_1)\rho_{2,N}^2 - (\chi_2 - \chi_1)\rho_{3,N}^2}{\chi_3 - \chi_2} \right)^{1/2}, \tag{4.11}$$

where $\rho_{2,N}$ and $\rho_{3,N}$ are given by equation (4.8$a$).

At $\chi = 1$ the function $\rho(\chi)$ also has singularity and respectively numerical value of $\rho_{N,N}$ from (4.8$b$) is not very accurate. To improve that accuracy we use that $\rho(1) = 1$ as found in Part II. Then using the trapezoidal rule we obtain much more accurate expression that

$$\rho(\chi_N) \simeq \rho_{N,N} = \frac{2\gamma_N}{1 - \chi_{N-1}}. \tag{4.12}$$

Figure 7 shows the density $\rho(\chi)$ for three different Stokes waves in log-log scaling. It is also seen that inside the branch cut and for small $\chi_c \ll 1$, the density $\rho(\chi)$ scales as $\chi^{2/3}$ which corresponds to the limiting Stokes wave. A deviation from that scaling occurs near $\chi = \chi_c$ and $\chi = 1$.

Classical Markov's theorem (Markoff 1895) proves pointwise convergence of the diagonal Padé approximants $[N/N]_f$ of the function $f$ of the type (4.5) with $\rho(\chi) \geqslant 0$ in the limit $N \rightarrow \infty$ for $\zeta \in \mathbb{C} \setminus [i\chi_c, i]$. Here the diagonal Padé approximation $[N/N]_f$ of the function $f$ means that both polynomials $P(\zeta)$ and $Q(\zeta)$ has the same order $N$ which is natural for the discretization (4.6). More general Padé approximants of the function $f$ are $[N/M]_f$, where $N$ and $M$ are the orders of the polynomials $P(\zeta)$ and $Q(\zeta)$, respectively. Theorem of de Montessus de Ballore (1902) ensures pointwise convergence of $[N/M]_f \rightarrow f$ for $N \rightarrow \infty$ with fixed $M$ in the disk $|\zeta| < R$ if $f$ the meromorphic function in that disk with exactly $M$ poles (counted according to their multiplicity). However, the diagonal Padé approximations of the meromorphic function $f$ generally fails to provide uniform convergence with the known counterexamples given by Buslaev (2001); Lubinsky (2003). Nuttall (1970) showed that instead the diagonal Padé approximants of meromorphic function for $N \rightarrow \infty$ have a weaker convergence in logarithmic
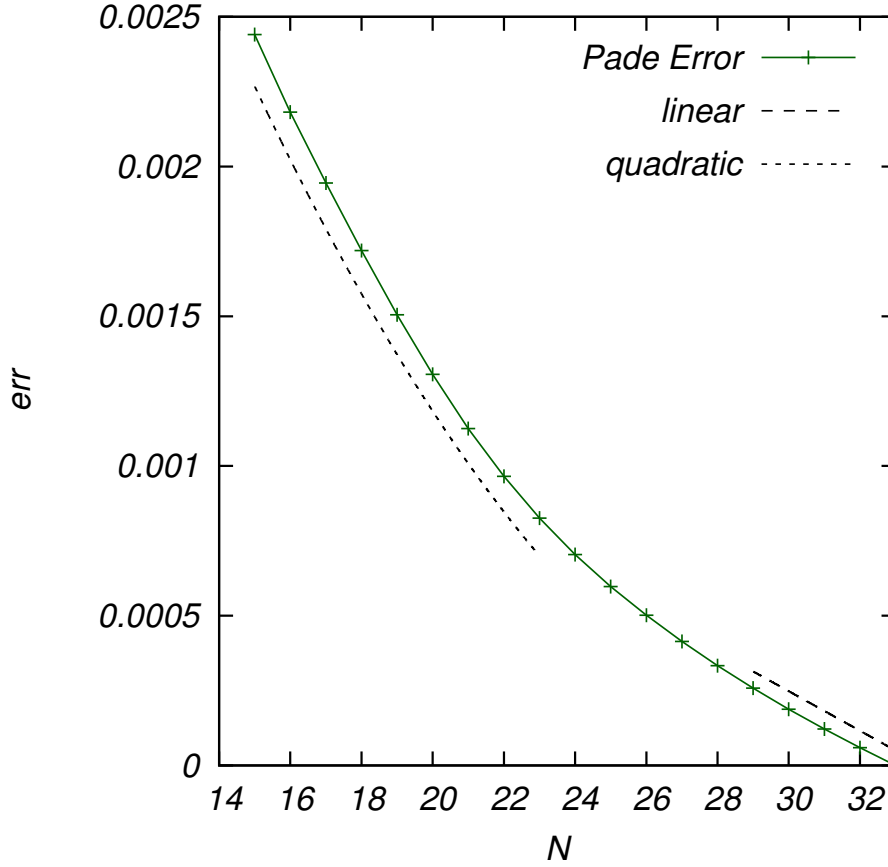
FIGURE 8. Error between Padé approximation with $N$ poles and the continuous limit for $\rho(\chi)$ for Stokes wave with $H/\lambda = 0.125510247666212033511898125908053$. It is seen that the error $\propto \frac{1}{N^2}$ for large $N$. To calculate that error we use a spline interpolation for $\rho^2_{n,N}$ with $N = N_{max} = 33$ to construct the approximation of the continuous limit of the square of the density, $\rho^2_{continuous}(\chi)$. After that the error is defined as err $\equiv \left( \sum_{n=2}^{N-1} [\rho^2_{n,N} - \rho^2_{continuous}(\chi_n)]^2 \right)^{1/2} / (N-2)$ for each $N$, where $\rho_{n,N}$ is given by equation (4.8).

capacity which allows the lack of pointwise convergence along exceptional sets. Gonchar (Gonchar 1973, 1975) extended Markov's theorem on the pointwise convergence of the diagonal Padé approximants to the functions $f + r$, where $f$ is the function of the type (4.5) with $\rho(\chi) > 0$ almost everywhere in $\chi \in [\chi_c, 1]$ and $r$ is the meromorphic function away from branch cut and has no poles at branch cut. Convergence in logarithmic capacity of the diagonal Padé approximants of the analytic function $f(\zeta)$ with a finite number of branch points (this is a more general type than the type (4.5) because these branch points can be located away from a single line) was proven by Stahl (1985$a$,$b$, 1997). That convergence occurs away from certain sets of $\mathbb{C}$ (in some cases these sets are simple arcs). See also Ref. Aptekarev *et al.* (2011) for the recent review. All these results were obtained for Padé approximants based on the Taylor series at a single point in $\mathbb{C}$. Thus these results do not directly apply to AGH algorithm which is based on least squares approximation at multiple points of $\mathbb{C}$. AGH algorithm is also distinct from multipoint Padé approximation (G. A. Baker & Graves-Morris 1996; Saff 1972), where the Taylor

series is interpolated at multiple points in contrast to least squares in AGH algorithm. Padé approximants were also constructed based on least squares in Ref. Gonnet *et al.* (2011) were it was conjectured that least squares-type algorithms might ensure pointwise convergence. That conjecture is consistent with our simulations.

### 4.3. *Finding a numerical value of a location of branch point $\zeta = i\chi_c$*

There are different ways to find the location of branch point $\zeta = i\chi_c$ from simulations. First way is based on the decay of Fourier spectrum of $\tilde{z}(\zeta)$ for $n \gg 1$ and is described in Section 3.3. Second way is to find $\rho(\chi_n)$, $n = 1, \ldots, N$ and then determine the point $\rho(\chi_c) = 0$ by the polynomial extrapolation of $\rho(\chi_n)$. First and second ways provide comparable numerical accuracy in our simulations (typically the relative error in $\chi_c$ is $\sim 10^{-4}$).

We found however, that better accuracy is achieved in the third way as follows. Consider the formal series

$$\tilde{z}_{ser} = \sum_{j=0}^{\infty} ie^{\mathrm{i}j\pi/4} a_j (\zeta - \mathrm{i}\chi_c)^{j/2} \tag{4.13}$$

in the neighborhood of the branch point $\zeta = \mathrm{i}\chi_c$. The term $ie^{\mathrm{i}j\pi/4}$ in front of the coefficients $a_j$ is chosen for convenience to ensure that coefficients $a_j$ take real values. The radius of convergence of that series is $2\chi_c$ as discussed in Part II. Taking $M = 10 - 20$ terms in that series one can use the nonlinear fit to determine the unknowns $\chi_c$ and $a_j$. Typically we use $N_j = 30 - 40$ points $(u_n, \tilde{z}(u_n))$ such that all values $u_n$ are inside the disk of convergence $|u_n - \mathrm{i}\chi_c| < 2\chi_c$ of the series (4.13). Here values of $\tilde{z}(u_n)$ are taken from simulations of Section 3 with $u_n$ being the numerical grid points closest to $u = 0$. The accuracy of the nonlinear fit is typically $\sim 10^{-10}$ as estimated by varying $M$ and $N_M$. In Part II we provide much more accurate way of calculating $\chi_c$ which is based on the compatibility of the series (4.13) with the equation (2.33) of Stokes wave. In contrast, the above three methods use numerical values of $(u_n, \tilde{z}(u_n))$ obtained as described in Section 3 and do not use the equation (2.33) directly.

## 5. Stokes wave as an integral over jump at branch cut and the expansion of density $\rho$ near a branch point

### 5.1. *Jump at branch cut*

Sokhotski-Plemelj theorem (see e.g. Gakhov (1966); Polyanin & Manzhirov (2008)) applied to the equation (4.5) gives

$$\tilde{z}(\mathrm{i}\chi \pm 0) = \mathrm{i}y_0 + \text{p.v.} \int_{\chi_c}^{1} \frac{\rho(\chi')\mathrm{d}\chi'}{\mathrm{i}(\chi - \chi')} \pm \pi\rho(\chi), \ \chi_c < \chi < 1. \tag{5.1}$$

Thus the jump of $\tilde{z}(\zeta)$ at branch cut is $-2\pi\rho(\chi)$ for crossing branch cut at $\zeta = \mathrm{i}\chi$ in counterclockwise direction.

### 5.2. *Stokes wave as the sum of contribution from branch cuts in $w$ complex plane*

Consider a representation of Stokes wave by the density $\tilde{\rho}$ along branch cuts in complex plane $w$. Because of the $2\pi$-periodicity in $u$ direction we write $z(w)$ as the integral over

periodically located branch cuts,

$$\tilde{z}(w) = z_1 + \int\limits_{v_c}^{\infty} \sum_{n=-\infty}^{\infty} \left( \frac{1}{w + 2\pi n - \mathrm{i}v'} - \frac{1}{b + 2\pi n - \mathrm{i}v'} \right) \tilde{\rho}(v')\mathrm{d}v', \qquad (5.2)$$

where $z_1$ is the complex constant, $v_c$ is related to $\chi_c$ by (4.2), a summation over $n$ ensure the periodicity of $\tilde{z}(w)$ along $u$ and we replaced $\rho(\chi)$ by $\tilde{\rho}(v')$ to distinguish it from $\rho(\chi)$ in (4.5). Also we introduced the additional term $-\dfrac{1}{b + 2\pi n - \mathrm{i}v'}$ which is intended to ensure the convergence of the integral. The constant $b$ can be chosen at our convenience. A change of that constant results in the change of $z_1$.

The sum in (5.2) is then calculated using of the identity

$$\sum_{n=-\infty}^{\infty} \frac{1}{n+a} = \pi \cot \pi a$$

giving

$$\tilde{z}(w) = z_1 + \frac{1}{2} \int\limits_{v_c}^{\infty} \left( \cot\left[\frac{w - \mathrm{i}v'}{2}\right] - \cot\left[\frac{b - \mathrm{i}v'}{2}\right] \right) \tilde{\rho}(v')\mathrm{d}v'. \qquad (5.3)$$

Taking the limit $Im(w) \to -\infty$ we obtain from equations (5.3) and (4.5) that

$$\tilde{z}(u - \mathrm{i}\infty) = z_1 + \frac{1}{2} \int\limits_{v_c}^{\infty} \left( \mathrm{i} - \cot\left[\frac{b - \mathrm{i}v'}{2}\right] \right) \tilde{\rho}(v')\mathrm{d}v' = \mathrm{i}y_0 + \int\limits_{\chi_c}^{1} \frac{\rho(\chi)\mathrm{d}\chi}{-\mathrm{i} - \mathrm{i}\chi}. \qquad (5.4)$$

We set

$$\chi = \tanh \frac{v'}{2} \qquad (5.5)$$

and

$$\rho(\chi) = \tilde{\rho}(2\operatorname{arctanh}\chi). \qquad (5.6)$$

We also require that $z_1 = \mathrm{i}y_0$ then we find from the equations (5.4), (5.5) and (5.6) that

$$b = \pi. \qquad (5.7)$$

Using the trigonometric identity

$$\cot(a - b) = \frac{1 + \tan a \tan b}{\tan a - \tan b}$$

one obtains from (5.3), (5.4), (5.5), (5.6) and (5.7) that

$$\tilde{z}(w) = \mathrm{i}y_0 + \frac{1}{2} \int\limits_{v_c}^{\infty} \left( \frac{\left[1 + \mathrm{i}\tan\frac{w}{2}\tanh\frac{v'}{2}\right]}{\tan\frac{w}{2} - \mathrm{i}\tanh\frac{v'}{2}} - \mathrm{i}\tanh\frac{v'}{2} \right) \tilde{\rho}(v')\mathrm{d}v'$$

$$= \mathrm{i}y_0 + \frac{1}{2} \int\limits_{v_c}^{\infty} \left( \frac{1 + \mathrm{i}\zeta\chi}{\zeta - \mathrm{i}\chi} - \mathrm{i}\chi \right) \tilde{\rho}(v')dv' = \mathrm{i}y_0 + \int\limits_{\chi_c}^{1} \frac{\rho(\chi)\mathrm{d}\chi}{\zeta - \mathrm{i}\chi}, \qquad (5.8)$$

i.e. we recovered the equation (4.5) from the equation (5.2).

### 5.3. *Expansion of $\rho(\chi)$ in powers of $\zeta - i\chi_c$*

Assume that we have the branch cut $(i\chi_c, i)$ for $z(\zeta)$ in the complex plane of $\zeta$ and that the branch point at $\zeta = i\chi_c$ is of square root type. Then we expand $\rho(\chi)$ in the following series

$$\rho(\chi) = \sum_{n=0}^{\infty} b_{2n+1}(\chi - \chi_c)^{1/2+n}. \tag{5.9}$$

Note that that adding terms of integer powers of $(\zeta - i\chi_c)$ into the equation (5.9) is not allowed because it would produce logarithmic singularity at $\zeta = i\chi_c$ through the equation (4.5) which is incompatible with the Stokes wave as was shown in Refs. Grant (1973); Tanveer (1991).

Integrating over $\chi$ in (4.5) using (5.9) gives

$$f(\zeta) = b_1 \left( 2i\sqrt{1-\chi_c} - 2i\sqrt{\chi_c + i\zeta} \arctan\left[\frac{\sqrt{1-\chi_c}}{\sqrt{\chi_c + i\zeta}}\right] \right)$$

$$+ b_3 \left( \frac{2}{3}\sqrt{1-\chi_c}(i - 4i\chi_c + 3\zeta) + 2i(\chi_c + i\zeta)^{3/2} \arctan\left[\frac{\sqrt{1-\chi_c}}{\sqrt{\chi_c + i\zeta}}\right] \right)$$

$$+ b_5 \left( \frac{2}{15}\sqrt{1-\chi_c} \left( 3i - 11i\chi_c + 23i\chi_c^2 + 5\zeta - 35\chi_c\zeta - 15i\zeta^2 \right) \right.$$

$$\left. -2i(\chi_c + i\zeta)^{5/2} \arctan\left[\frac{\sqrt{1-\chi_c}}{\sqrt{\chi_c + i\zeta}}\right] \right) + b_7(\ldots) + \ldots \tag{5.10}$$

A series expansion of (5.10) at $\zeta = i\chi_c$ and comparison with the series (4.13) result in the relations

$$b_{2j+1} = (-1)^{j+1}a_{2j+1}, \ j = 0, 1, 2, \ldots \tag{5.11}$$

Note that the expansion (5.10) provides the relations for $b_n$ with only odd values of $n$. This is because the series (5.9) is convergent only inside its disk of convergence, $\chi - \chi_c < r$, where $r$ is the radius of convergence. It will be shown in Part II that $r = 2\chi_c$ for $\chi_c < 1/3$. The explicit expression for $\rho(\chi)$ is unknown for $\chi_c + r < \chi < 1$ while $\rho(\chi)$ still contributes to the terms $a_{2j}(\zeta - i\chi_c)^j$, $j = 0, 1, 2, \ldots$ in the series (4.13).

Thus the expansion (5.9) together with the relations (5.11) provides a convenient tool to work with $\rho(\chi)$ near to $\chi = \chi_c$.

### 5.4. *Absence of singularities in branch cut beyond the branch points $\zeta = i\chi_c$ and $\zeta = i$.*

A priori one can not exclude existence of singularities inside the branch cut $\zeta \in [i\chi_c, i]$ beyond branch points $\zeta = i\chi_c$ and $\zeta = i$ at its ends. Existence of such singularities were conjectured in Refs. Grant (1973); Schwartz (1974). To address that possibility we subtracted the expansion (5.10) from the numerical solution of $\tilde{z}(\zeta)$ for Stokes wave. We obtained both $\tilde{z}(\zeta)$ and recovered $\rho(\chi)$ through AGH algorithm using variable precision arithmetics with $\sim 200$ digits to achieve a high precision in that subtraction. Typically we used Stokes wave of the moderate nonlinearity with $\chi_c \sim 10^{-2}$ to operate with the moderate number of required Fourier harmonics. After that the numerical values of $b_1, b_3, b_5, \ldots$ were recovered from fitting of $\rho(\chi)$ to the expansion (5.9) near $\chi = \chi_c$. Typically we truncated the expansion (5.9) to the first 3 terms $b_1, b_3, b_5$ which results in the truncated function $f(\zeta)_{truncated}$ in the expansion (5.10). Also $\chi_c$ was obtained by the procedures described in Section 4.3. Alternative way to recover $b_1, b_3, b_5$ is through using the expansion (3.4) was also used but generally gives lower precision.

Next step was to take $m$th derivative of $\tilde{z}(\zeta) - f(\zeta)_{truncated}$ over $\zeta$ numerically and

obtain the Padé approximation for the resulting expression $[\tilde{z}(\zeta) - f(\zeta)_{truncated}]^{(m)}$ resulting in new density $\tilde{\rho}(\chi)$. If any singularity would be present inside the branch cut then it would correspond to singularity in $\tilde{\rho}(\chi)$. However, we did not find any sign of such singularities at least for moderate order of derivative $m = 1, 2, 3$. It suggests that $\zeta = i\chi_c$ and $\zeta = i$ are the only singularities in complex $\zeta$ plain. This conclusion is in agreement with the results of both Tanveer (1991) and Part II obtained by alternative methods.

## 6. Conclusion

In this paper we found numerically the Stokes solutions of the primordial Euler equations with free surface for large range of wave heights, including the approach to the limiting Stokes wave. The limiting Stokes wave emerges as the singularity reaches the fluid surface. We found from our high precision simulations (between 32 and more than 200 digits) the Padé approximation of branch cut singularity of Stokes wave. We provided the tables of the Padé approximants for a wide range of Stokes wave steepness. These tables allow to recover Stokes wave with the minimum accuracy $10^{-26}$. We show that these Padé approximants quickly converge to the jump at branch cut as the number of poles $N$ increases with the scaling law (4.3),(4.4). We use the series expansion of the jump along branch cuts in half integer powers to recover the square-root singularity at the branch point. We found that there are no more singularities in the finite complex plane beyond one branch point per period. Following Part II is devoted to the analysis of the structure and location of branch points in infinite set of sheets of Riemann surface beyond the physical sheet of Riemann surface considered here.

## Appendix A. Derivation of dynamical equations

In this Appendix we adapt the work of Dyachenko *et al.* (1996*a*) to the case of the periodic boundary conditions deriving the basic dynamical equations (2.10) and (2.11) for 2D ideal hydrodynamics with free surface in conformal variables. We use similar notations to Dyachenko *et al.* (1996*a*) and provide steps of the derivation skipped in Dyachenko *et al.* (1996*a*).

### A.1. *Hamiltonian after conformal map*

It was shown by Zakharov (1968), that the potential flow of an ideal fluid with free surface is the canonical Hamiltonian system with canonical variables $\eta$ (2.4) and $\psi$ (2.5). Canonical Hamiltonian equations

$$\frac{\partial \eta}{\partial t} = \frac{\delta H}{\delta \psi}, \ \ \frac{\partial \psi}{\partial t} = -\frac{\delta H}{\delta \eta}. \tag{A 1}$$

are equivalent to the boundary conditions (2.2) and (2.3). Here $H$ is the Hamiltonian which coincides with the total energy (the sum of the kinetic energy $T$ and the potential
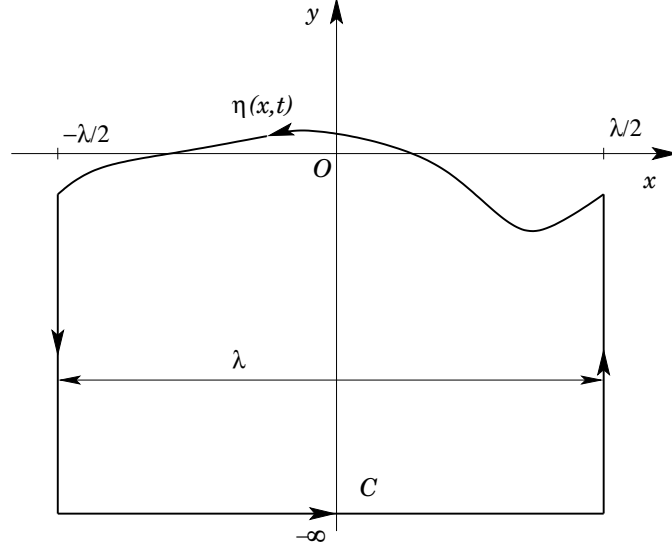
FIGURE 9. A schematic of one period of a wave with a counterclockwise contour of integration for application of Green's theorem.

energy $U$) per spatial period of wave $\lambda$,

$$H = T + U = \frac{1}{2} \int\limits_{-\lambda/2}^{\lambda/2} \mathrm{d}x \int\limits_{-\infty}^{\eta} (\nabla\Phi)^2 \mathrm{d}y + \frac{g}{2} \int\limits_{-\lambda/2}^{\lambda/2} \eta^2 \mathrm{d}x,$$

and without loss of generality the fluid density is set to one. One has to express the kinetic energy

$$T = \frac{1}{2} \int\limits_{-\lambda/2}^{\lambda/2} \mathrm{d}x \int\limits_{-\infty}^{\eta} (\nabla\Phi)^2 \mathrm{d}y \qquad (A\,2)$$

through the canonical variables $\eta$ and $\psi$ which generally requires to solve the Laplace equation (2.1) with the boundary conditions (2.2), (2.3), (2.5) and $\Phi(x, y, t)|_{y\to-\infty} = 0$ in the region $-\frac{\lambda}{2} \leqslant x < \frac{\lambda}{2}$, $-\infty < y \leqslant \eta(x, t)$. That region is schematically shown in Figure 9. Using relations

$$\nabla \cdot (\Phi\nabla\Phi) = (\nabla\Phi)^2 + \Phi\nabla^2\Phi, \quad (\nabla\Phi)^2 = \frac{\partial}{\partial x}\left(\Phi\frac{\partial\Phi}{\partial x}\right) + \frac{\partial}{\partial y}\left(\Phi\frac{\partial\Phi}{\partial y}\right),$$

which are valid for the harmonic function $\Phi$ (2.1) and applying Green's theorem to the equation (A 2) one obtains that

$$2T = \int\limits_{-\lambda/2}^{\lambda/2} \int\limits_{-\infty}^{\eta} \left\{ \frac{\partial}{\partial x}\left(\Phi\frac{\partial\Phi}{\partial x}\right) + \frac{\partial}{\partial y}\left(\Phi\frac{\partial\Phi}{\partial y}\right) \right\} \mathrm{d}x\mathrm{d}y = \int\limits_{C} \left( -\Phi\frac{\partial\Phi}{\partial y}\mathrm{d}x + \Phi\frac{\partial\Phi}{\partial x}\mathrm{d}y \right). \quad (A\,3)$$

Here $C$ is a positively (counterclockwise) oriented contour along the boundary of the periodic domain occupied by fluid shown in Figure 9. A sum of integrals along left and right hand sides (vertical segments) of the contour vanishes due to periodicity. Integral along lower part of the contour (horizontal segment) is zero due to the boundary condition on potential $\Phi_{y=-\infty} = 0$. Notice that in the case of finite depth fluid with a rigid flat

bottom $y = -h$, the integral along similar lower segment $y = -h$ is also zero because the boundary condition at the finite depth bottom is $\Phi_y|_{y=-h} = 0$ (zero vertical velocity at the bottom) and $\mathrm{d}y = 0$. Then the equation (A 3) is reduced to the following line integral

$$2T = \int\limits_{x=\lambda/2,\ y=\eta(x,t)}^{x=-\lambda/2} \left( -\Phi \frac{\partial \Phi}{\partial y} \mathrm{d}x + \Phi \frac{\partial \Phi}{\partial x} \mathrm{d}y \right). \qquad (A\,4)$$

We use the time-dependent conformal transformation (2.6),(2.7) to relate partial derivatives in $x, y$ and $u, v$ as follows

$$\frac{\partial \Phi}{\partial u} = \frac{\partial \Phi}{\partial x} x_u + \frac{\partial \Phi}{\partial y} y_u,$$

$$\frac{\partial \Phi}{\partial v} = \frac{\partial \Phi}{\partial x} x_v + \frac{\partial \Phi}{\partial y} y_v,$$

which implies that

$$\frac{\partial \Phi}{\partial x} = \frac{\Phi_u x_u - \Phi_v y_u}{x_u^2 + y_u^2}, \qquad (A\,5)$$

$$\frac{\partial \Phi}{\partial y} = \frac{\Phi_u y_u + \Phi_v x_u}{x_u^2 + y_u^2}, \qquad (A\,6)$$

where we also used Cauchy-Riemann equations $x_u = y_v$ and $x_v = -y_u$ for the conformal map $z(w)$.

Substituting (A 5) and (A 6) into (A 4), using relations $\mathrm{d}x = x_u \mathrm{d}u$ and $\mathrm{d}y = y_u \mathrm{d}u$ on the line $w = u$ one obtains that

$$2T = \int\limits_{\lambda/2}^{-\lambda/2} (-\Phi_v \Phi)|_{v=0} \,\mathrm{d}u = \int\limits_{-\lambda/2}^{\lambda/2} \Phi_v \Phi|_{v=0} \,\mathrm{d}u. \qquad (A\,7)$$

Here we took into account the orientation of the contour and conditions (2.7) on conformal transformation.

Sokhotski-Plemelj theorem (5.1) (see e.g. Gakhov (1966); Polyanin & Manzhirov (2008)) allows to express a real part of the function which is analytic in the lower (upper) half plane through the imaginary part (and vice versa) at the real line $u = w$ using the Hilbert transformation (2.12). For a conformal transformation $z(w,t) = x(w,t) + \mathrm{i}y(w,t)$ such relations are given by (2.29). A complex velocity potential $\Pi(z,t) = \Phi + \mathrm{i}\Theta$ is the analytic function in the fluid domain $-\infty < y \leqslant \eta(x,t)$, where $\Theta$ is the stream function. The conformal transformation $z = z(w,t)$ (2.6) ensures that $\Pi$ remains analytic function after transforming from $z$ to $w$ variable with the lower half plane $\mathbb{C}^-$ being the domain of analyticity in $w$. Similar to equation (2.29), real and imaginary parts of $\Pi$ are related at the real line $u = w$ through the Hilbert transformation as follows

$$\Theta = \hat{H}\Phi, \quad \Phi = -\hat{H}\Theta, \qquad (A\,8)$$

where we assumed the decaying boundary condition $\Phi|_{v=-\infty} = \Theta|_{v=-\infty} = 0$. Here we abuse notation and use the same $\Pi$ and $\Phi$ both for independent variables $w$ and $z$ : $\tilde{\Phi}(w,t) \equiv \Phi(z,t)$ and $\tilde{\Pi}(w,t) \equiv \Pi(z,t)$, i.e. we omit tilde.

Also the analyticity of $\Pi$ implies that the velocity potential $\Phi$ is the harmonic function satisfying the Laplace equation (2.1) both in $x, y$ variables and similarly

$$\nabla^2 \Phi(u, v, t) = 0$$

in variables $u$ and $v$. Using Cauchy-Riemann equations (2.15) and the relations (A 8) one obtains that

$$\Phi_v = -\hat{H}\Phi_u. \tag{A 9}$$

Substituting (A 9) into (A 7) we express the kinetic energy in terms of canonical variable $\psi$ as follows

$$2T = \int\limits_{-\lambda/2}^{\lambda/2} \Phi_v\Phi|_{v=0}\, \mathrm{d}u = -\int\limits_{-\lambda/2}^{\lambda/2} \psi\hat{H}\psi_u\mathrm{d}u, \tag{A 10}$$

Here we used the definition (2.5) which in $w$ plane turns into $\psi(u,t) \equiv \Phi(u, v = 0, t)$ as follows from the mapping of the fluid surface into the real line $v = 0$. Then the Hamiltonian in terms of variables on the surface takes the following form

$$H = -\frac{1}{2}\int\limits_{-\lambda/2}^{\lambda/2} \psi\hat{H}\psi_u\mathrm{d}u + \frac{g}{2}\int\limits_{-\lambda/2}^{\lambda/2} y^2 x_u\mathrm{d}u. \tag{A 11}$$

### A.2. *Least action principle in conformal variables*

We use the constrained Lagrangian formulation to obtain the dynamical equations in conformal variables at fluid surface. A time dependence of the map (2.6) implies that we have to ensure the analyticity of that map through the appropriate constraint. We discuss the Lagrangian dynamics first and add the corresponding constraint later in this Section. Equations (A 1) realize extremum of an action

$$S = \int\limits_{t_1}^{t_2} L\mathrm{d}t, \tag{A 12}$$

with the Lagrangian

$$L = \int\limits_{-\lambda/2}^{\lambda/2} \psi\frac{\partial\eta}{\partial t}\mathrm{d}x - H. \tag{A 13}$$

The first term here has to be converted from the integral over $x$ into $u$ variable. Consider mapping $(x, t) \to (u, \tau)$, which is the change of parametrization of the surface under the conformal map. Here $\tau = t$. Transformation $u = u(x, t)$ is the inverse to the conformal map $x = x(u, \tau)$. The fluid surface $\eta(x, t)$ after transformation corresponds to $y(u, \tau)$. We express $\partial\eta/\partial t$ by the chain rule as follows

$$\frac{\partial\eta}{\partial t} = \frac{\partial y}{\partial\tau}\frac{\partial\tau}{\partial t} + \frac{\partial y}{\partial u}\frac{\partial u}{\partial t} = \frac{\partial y}{\partial\tau} + \frac{\partial y}{\partial u}\frac{\partial u}{\partial t}. \tag{A 14}$$

To find $\partial u/\partial t$ here we express full differentials of $x$ and $t$ through $u$ and $\tau$ as follows

$$\begin{pmatrix} \mathrm{d}x \\ \mathrm{d}t \end{pmatrix} = \begin{pmatrix} x_u & x_\tau \\ t_u & t_\tau \end{pmatrix}\begin{pmatrix} \mathrm{d}u \\ \mathrm{d}\tau \end{pmatrix} \equiv J\begin{pmatrix} \mathrm{d}u \\ \mathrm{d}\tau \end{pmatrix}. \tag{A 15}$$

Taking into account that $\tau = t$, one obtains the Jacobian matrix

$$J = \begin{pmatrix} x_u & x_\tau \\ 0 & 1 \end{pmatrix}. \tag{A 16}$$

Inverse procedure for full differentials of $u$ and $\tau$ through $x$ and $t$ yields that

$$\left( \begin{array}{c} \mathrm{d}u \\ \mathrm{d}\tau \end{array} \right) = \left( \begin{array}{cc} \partial u/\partial x & \partial u/\partial t \\ \partial \tau/\partial x & \partial \tau/\partial t \end{array} \right) \left( \begin{array}{c} \mathrm{d}x \\ \mathrm{d}t \end{array} \right) = J^{-1} \left( \begin{array}{c} \mathrm{d}x \\ \mathrm{d}t \end{array} \right). \tag{A 17}$$

Comparing entries of the matrix in (A 17) with inverse of (A 16), one gets

$$\frac{\partial u}{\partial t} = -\frac{x_\tau}{x_u}. \tag{A 18}$$

Substituting (A 18) into (A 14) yields

$$\frac{\partial \eta}{\partial t} = y_\tau - y_u \frac{x_\tau}{x_u}. \tag{A 19}$$

We use the Lagrangian (A 13) to substitute it into the action (A 12). Consider the first term in the action,

$$S = \int \int L \mathrm{d}t = \int \int \psi \frac{\partial \eta}{\partial t} \mathrm{d}x \mathrm{d}t + \dots \tag{A 20}$$

and perform a change of variables in the integral as $\mathrm{d}x\mathrm{d}t = \det(J)\mathrm{d}u\mathrm{d}\tau = x_u \mathrm{d}u\mathrm{d}\tau$. Together with the expression (A 19) it results in

$$\int \int \psi \frac{\partial \eta}{\partial t} \mathrm{d}x\mathrm{d}t = \int \int \psi \left( y_\tau - y_u \frac{x_\tau}{x_u} \right) x_u \mathrm{d}u\mathrm{d}\tau = \int \int \psi(y_\tau x_u - y_u x_\tau)\mathrm{d}u\mathrm{d}\tau. \tag{A 21}$$

Using (A 11), (A 13), (A 21) and adding the analyticity constraint (2.29) ensuring that $\tilde{y} - y_0 = \hat{H}\tilde{x}$ and taking into account that $\tau = t$ as well we obtain a new constrained Lagrangian

$$L = \int_{-\lambda/2}^{\lambda/2} \psi(y_t x_u - y_u x_t)\mathrm{d}u + \frac{1}{2} \int_{-\lambda/2}^{\lambda/2} \psi \hat{H}\psi_u \mathrm{d}u - \frac{g}{2} \int_{-\lambda/2}^{\lambda/2} y^2 x_u \mathrm{d}u \tag{A 22}$$

$$+ \int_{-\lambda/2}^{\lambda/2} (y - \tilde{y}_0 - \hat{H}\tilde{x})f\mathrm{d}u,$$

where $f$ is the Lagrange multiplier for the analyticity constraint.

### A.3. *Variations of action*

We now obtain the dynamical equations from the Hamilton's least action principle. Vanishing of variational derivative $\delta S/\delta \psi = 0$ of the action (A 12) with the Lagrangian (A 22) over potential $\psi$ on the surface yields the following expression

$$y_t x_u - y_u x_t + \hat{H}\psi_u = 0. \tag{A 23}$$

This equation is nothing else but kinematic boundary condition (2.2) after the conformal map into $w$ plane.

Two conditions $\delta S/\delta x = 0$ and $\delta S/\delta y = 0$ result in equations

$$y_u \psi_t - y_t \psi_u + gyy_u = \hat{H}f, \tag{A 24}$$
$$-x_u \psi_t + x_t \psi_u - gyx_u = f, \tag{A 25}$$

which are turned into a single equation by excluding the Lagrange multiplier $f$ giving

$$y_u \psi_t - y_t \psi_u + \hat{H}(x_u \psi_t - x_t \psi_u) + g[yy_u + \hat{H}(yx_u)] = 0. \tag{A 26}$$

Equations (A 23) and (A 26) recover the implicit dynamical equations (2.10) and (2.11).

A.4. *Zeroth harmonic in implicit dynamical equations* (2.10) *and* (2.11) *and*
*conservation of momentum*

Consider Fourier transformations of the surface elevation $y(u,t)$ and the velocity potential on surface $\psi$ with respect to conformal coordinate $u$,

$$
\begin{aligned}
y(u,t) &= y_0(t) + \sum_{k\neq 0} y_k(t)\mathrm{e}^{\mathrm{i}ku}, \\
\psi(u,t) &= \psi_0(t) + \sum_{k\neq 0} \psi_k(t)\mathrm{e}^{\mathrm{i}ku}.
\end{aligned}
\tag{A 27}
$$

Here zeroth harmonics $y_0(t)$ and $\psi_0(t)$ are written separately and are given by

$$
y_0(t) = \frac{1}{\lambda}\int_{-\lambda/2}^{\lambda/2} y(u,t)\mathrm{d}u, \quad \psi_0(t) = \frac{1}{\lambda}\int_{-\lambda/2}^{\lambda/2}\psi(u,t)\mathrm{d}u.
\tag{A 28}
$$

One can rewrite equation (A 26) in the following form

$$
y_u\psi_t - y_t\psi_u = -\hat{H}(x_u\psi_t - x_t\psi_u + yx_u) - \frac{g}{2}\frac{\partial}{\partial u}y^2.
\tag{A 29}
$$

A zeroth Fourier harmonic of the right hand side (r.h.s.) of equation (A 29) vanishes because the term in parenthesis is multiplied by $\hat{H}$ which removes any zeroth harmonic and the remaining term is the partial derivative over $u$. Respectively, the zeroth harmonic of the left hand side (l.h.s.) of equation (A 29) must vanish. Integrating that l.h.s. to obtain the zeroth harmonic, using equation (A 29) and integrating by parts over $u$ one obtains that

$$
\frac{1}{\lambda}\int_{-\lambda/2}^{\lambda/2}(y_u\psi_t - y_t\psi_u)\mathrm{d}u = \frac{1}{\lambda}\int_{-\lambda/2}^{\lambda/2}(y_u\psi_t + y_{ut}\psi)\mathrm{d}u = \frac{1}{\lambda}\frac{\partial}{\partial t}\int_{-\lambda/2}^{\lambda/2}\psi y_u\mathrm{d}u = 0,
\tag{A 30}
$$

where we used a periodicity of $\psi$ and $y$ in $u$. Thus $\int_{-\lambda/2}^{\lambda/2}\psi y_u\mathrm{d}u$ is the integral of motion. To find a physical meaning of that integral we note that natural candidates for conserved quantities are the components of the total momentum of fluid along $x$ and $y$ directions. Taking into account that fluid density is one, we obtain $x$ component of momentum $P_x$ as an integral of the horizontal velocity inside fluid, which gives

$$
P_x = \int_{-\lambda/2}^{\lambda/2}\mathrm{d}x\int_{-\infty}^{\eta(x,t)}\Phi_x\mathrm{d}y = \int_C\Phi\mathrm{d}y = \int_{\lambda/2}^{-\lambda/2}\Phi\left.\frac{\partial y}{\partial x}\right|_{y=\eta(x,t)}\mathrm{d}x = -\int_{-\lambda/2}^{\lambda/2}\psi y_u\mathrm{d}u.
\tag{A 31}
$$

Here we applied Green's theorem to positively oriented contour $C$ shown in Figure 9. Due to periodicity of functions and decaying boundary condition $\Phi(x,y,t)|_{y\to-\infty} = 0$, only integral along the surface is nonzero. Comparison of equations (A 30) and (A 31) shows that consistency of equation (A 29) is ensured by the conservation of the horizontal component $P_x$ of the total momentum of the fluid.

Applying the Hilbert transformation $\hat{H}$ to equation (A 29) and using the identity (2.28) one obtains that

$$
x_u\psi_t - x_t\psi_u + yx_u - q_0 = \hat{H}\left(y_u\psi_t - y_t\psi_u + \frac{g}{2}\frac{\partial}{\partial u}y^2\right),
\tag{A 32}
$$

where $q_0$ is the zeroth Fourier harmonic of $x_u\psi_t - x_t\psi_u + yx_u$. To find $q_0$ we proceed

similar to equations (A 30) and (A 31) to find that

$$q_0 = \frac{1}{\lambda} \int\limits_{-\lambda/2}^{\lambda/2} (x_u \psi_t - x_t \psi_u + y x_u) \mathrm{d}u = \frac{1}{\lambda} \frac{\partial}{\partial t} \int\limits_{-\lambda/2}^{\lambda/2} \psi x_u \mathrm{d}u + \frac{1}{\lambda} \int\limits_{-\lambda/2}^{\lambda/2} y x_u \mathrm{d}u, \qquad (A\,33)$$

where $\int\limits_{-\lambda/2}^{\lambda/2} \psi x_u \mathrm{d}u$ is the integral of motion corresponding to the conservation of the vertical component $P_y$ of the total momentum of fluid,

$$P_y = \int\limits_{-\lambda/2}^{\lambda/2} \mathrm{d}x \int\limits_{-\infty}^{\eta(x,t)} \Phi_y \mathrm{d}y = \int\limits_{C} -\Phi \mathrm{d}x = \int\limits_{-\lambda/2}^{\lambda/2} \psi x_u \mathrm{d}u. \qquad (A\,34)$$

Then equations (A 33) and (A 34) imply that $q_0$ is the integral of motion given by

$$q_0 = \frac{1}{\lambda} \int\limits_{-\lambda/2}^{\lambda/2} y x_u \mathrm{d}u = \frac{1}{\lambda} \int\limits_{-\lambda/2}^{\lambda/2} \eta(x,t) \mathrm{d}x \qquad (A\,35)$$

and representing a conservation of the total mass of fluid. Also according to equation (2.17), we set $q_0 = 0$ in this paper.

## Appendix B. Alpert-Greengard-Hagstrom (AGH) Algorithm and Stokes Wave

In this Appendix we describe an efficient algorithm for Padé approximation of the function on a discrete grid, following original work Alpert *et al.* (2000) and work by Lau (2004) where more detailed explanation and further development of the algorithm was presented.

Consider $2\pi$-periodic complex-valued function $f(u) = z(u) - u - \mathrm{i}y_0$ defined on a grid with nodes $u_j \in [-\pi, \pi]$. Values of the function at the grid points are denoted as $f_j = f(u_j)$. We look for an approximation of $f(u)$ in the form of a ratio of two polynomials $P(u)$ and $Q(u)$, i.e. the Padé approximation. We briefly describe AGH algorithm in a general way with additional comments for our particular case. As it was mentioned in Section 4, we use the second conformal map $\zeta = \tan(u/2)$. The introduction of auxiliary variable $\zeta$ allows to consider the real line $\zeta \in \mathbb{R}$ as opposed to considering a finite interval $u \in [-\pi, \pi]$, while the infinity along the imaginary axis is mapped into imaginary unit i and $2\pi$-periodicity in $u$ direction is ensured. Without loss of generality we assume that $f(\pm\pi) = 0$. In this paper, we take $f(u) = z(u) - u - \mathrm{i}y_0 = \tilde{z}(u) - \mathrm{i}y_0$ (see equations (4.5) and (4.6) for comparison). Condition $f(\pm\pi) = 0$ allows to consider $P$ and $Q$ such that the degree of polynomials are $\deg Q = 1 + \deg P = N$, where the integer $N$ is allowed to vary. We are looking for the convergence of the rational approximation to $f$,

$$\frac{P(\zeta)}{Q(\zeta)} \to f(\zeta),$$

in a sense of solving a minimization problem

$$\min_{P,Q} \int\limits_{-\pi}^{+\pi} \left| \frac{P(u)}{Q(u)} - f(u) \right|^2 \mathrm{d}u. \qquad (B\,1)$$

That minimization problem is challenging because $Q$ in the denominator makes (B 1) nonlinear problem. In the transformed variable $\zeta$ the problem (B 1) remains nonlinear and is reduced to

$$\min_{P,Q} \int_{-\infty}^{+\infty} \left| \frac{P(\zeta)}{Q(\zeta)} - f(\zeta) \right|^2 \frac{\mathrm{d}\zeta}{\zeta^2 + 1}. \tag{B 2}$$

In AGH algorithm, the complexity of nonlinearity is bypassed by solving instead of (B 1), a sequence of linear least-square problems

$$\min_{P^{(i+1)}, Q^{(i+1)}} \int_{-\infty}^{+\infty} \left| \frac{P^{(i+1)}(u)}{Q^{(i)}(u)} - \frac{Q^{(i+1)}(u)}{Q^{(i)}(u)} f(u) \right|^2 \mathrm{d}u, \ i = 1, 2, \ldots \tag{B 3}$$

We define an inner product

$$\langle f, g \rangle_i = \int_{-\infty}^{+\infty} f(u) \bar{g}(u) w_i(u) \mathrm{d}u, \tag{B 4}$$

with a weight function $w_i(u) = \frac{1}{|Q^{(i)}(u)|^2}$ (for $\zeta$-plane the formula for the weight is modified to be $w_i(\zeta) = 1/(|Q^{(i)}(\zeta)|^2(\zeta^2 + 1))$). Then the previous least squares problem can be rewritten as follows

$$\min_{P^{(i+1)}, Q^{(i+1)}} || - P^{(i+1)}(u) + Q^{(i+1)}(u) f(u)||_i, \tag{B 5}$$

where

$$||g(u)||_i^2 = \langle g, g \rangle_i$$

is the norm.

As it was shown in Alpert *et al.* (2000), the solution of the least squares problem (B 5) is equivalent to the solution of

$$\langle -P^{i+1} + Q^{i+1} f(u), h_n(u) \rangle_i = 0,$$

for $n = 1, \ldots, 2N$, with $h_n(u)$ defined as follows

$$\begin{cases} u^{n/2-1}, & \text{for } n = 2, 4, 6, \ldots, 2N, \\ u^{(n-1)/2} f(u), & \text{for } n = 1, 3, 5, \ldots, 2N - 1, \end{cases} \tag{B 6}$$

which are nothing else but

$$f(u), 1, uf(u), u, u^2 f(u), \ldots, u^{N-1} f(u), u^{N-1}, u^N f(u).$$

This claim can be proven by variation of $m$th coefficient of $P(u)$ (for even $n = 2m + 2$) and $Q(u)$ (for odd $n = 2m + 1$). We put coefficient at the leading power of $Q(u)$ to be equal to one. Thus we need to find $2N$ coefficients for two polynomials.

We orthogonalize $2N + 1$ functions $h_n(u)$ using Gramm-Schmidt orthogonalization procedure,

$$g_n(u) = \begin{cases} f(u), & \text{for } n = 1, \\ 1 - c_{21} f(u), & \text{for } n = 2, \\ ug_{n-2}(u) - \sum_{j=1}^{\min\{4, n-1\}} c_{nj} g_{n-j}(u), & \text{for } n = 3, \ldots, 2N + 1, \end{cases} \tag{B 7}$$

where real constants $c_{nj}$ are given by

$$c_{nj} = \begin{cases} \frac{\langle 1, f(u) \rangle_i}{\langle f(u), f(u) \rangle_i}, & \text{for } n = 2 \text{ and } j = 1, \\ \frac{\langle (u g_{n-2}, g_{n-j} \rangle_i}{\langle g_{n-j}, g_{n-j} \rangle_i}, & \text{for } n = 3, \ldots, 2N+1 \text{ and } j = 1, \ldots, \min\{4, n-1\}. \end{cases} \quad \text{(B 8)}$$

Then we obtain that

$$g_{2N+1} = -P^{(i+1)} + f(u) Q^{(i+1)}, \quad \text{(B 9)}$$

so $P^{(i+1)}$ and $Q^{(i+1)}$ are computed from recurrence coefficients $c_{nj}$ by splitting into even and odd-numbered parts.

For our purposes of finding the jump at branch cut it is convenient to represent a ratio of $P(u)$ and $Q(u)$ as a sum of simple poles,

$$\frac{P(u)}{Q(u)} = \sum_{n=1}^{N} \frac{\gamma_n}{u - \chi_n}. \quad \text{(B 10)}$$

In order to do that we compute zeros $\chi_n$, $n = 1, 2, \ldots, N$ of $Q(u)$ using Newton's iterations. At each step one zero $\chi_n$ is found by Newton's iterations. After that we remove that zero from $Q(u)$ by division on $(u - \chi_n)$ and proceed to the next step for the modified $Q$ etc. After that procedure coefficients $\gamma_n$ are given by the following expression

$$\gamma_n = \frac{P(\chi_n)}{Q'(\chi_n)}. \quad \text{(B 11)}$$

Derivative $Q'(u)$ are obtained from previous recurrence relation for $g_n(u)$ by differentiation.

## Appendix C. Tables of Stokes Waves

Using the Padé approximation, introduced in Section 4, one can approximate Stokes wave for each value of the scaled height $H/\lambda$ as a sum of poles

$$z(w) \simeq z_{pade}(u) \equiv w + \mathrm{i}y_0 + \sum_{n=1}^{N} \frac{\gamma_n}{\tan(w/2) - \mathrm{i}\chi_n}. \quad \text{(C 1)}$$

Here $N$ is the number of poles in the Padé approximation. Using AGH algorithm (see Appendix B) we found that all poles for all values of $H/\lambda$ are located on the imaginary axis.

We provide Tables 1-4 for four particular cases of Stokes waves with wave heights ranging from $H/L \simeq 0.031791$ to $H/L \simeq 0.141058$. Complete library of computed waves can be accessed through the electronic attachments as well as through the web link Dyachenko *et al.* (2015). These data of Padé approximation allow to recover the Stokes wave with the relative accuracy of at least $10^{-26}$ (for the vast majority of cases the actual accuracy is higher by several orders of magnitude). First and second columns of both Tables and electronic files represent values of $\chi_n$ and $\gamma_n$, respectively. Additionally a third column in electronic files provides the values of $\rho_{n,N}$, $n = 1, 2, \ldots, N$ calculated from data of the first two columns using equations (4.8$a$), (4.11) and (4.12).

We used three quantities to characterize the accuracy of our numerical Stokes wave solution and its Padé approximation. First quantity is the residue

$$R(y) \equiv N^{-1/2} \left( \sum_{j=1}^{M} |\hat{L}_0 y(u_j)|^2 \right)^{1/2}$$

of equation (2.33). $R(y)$ characterizes convergence of our iteration algorithm described in Section 3.1 to the Stokes wave. Here $M = 2k_{max}$ is the number of grid points $u_j$ used in the discretization of $z(u)$. Second quantity is the relative error of Padé approximation

$$err_{pade} = \left( \frac{\sum\limits_{j=1}^{M} |z(u_j) - z_{pade}(u_j)|^2}{\sum\limits_{j=1}^{M} |z(u_j)|^2} \right)^{1/2}$$

of our numerical solution $z(u_j)$. Third quantity is the amplitude of the highest Fourier harmonics $|\hat{z}_{k_{max}}|$ used in FFT.

We balanced these three quantities in our simulation to achieve the most efficient and reliable approximants of Stokes waves. Typically we chose $k_{max}$ large enough such that $|\hat{z}_{k_{max}}| < M^{-1/2}10^{-26}$ to ensure that our discretization error is below $10^{-26}$. Here the factor $M^{-1/2}$ characterize the accumulation of round-off error in FFTs. A convergence of numerical iterations down to $R(y) \simeq 10^{-28}$ was found to be sufficient to achieve the desired accuracy of solution in $10^{-26}$. After that we used AGH algorithm with $N$ large enough to make sure that $err_{pade}$ is below $10^{-26}$ by several orders of magnitude.

The second and third rows in electronic `.dat`-files provide the additional information extracted from simulations which include the number of points of the numerical grid $M = 2k_{max}$, the residual $R(y)$, the Stokes wave height $y_0$ at $x = \pm\pi$, the amplitude of the highest Fourier harmonics $|\hat{z}_{k_{max}}|$, the Padé error $err_{pade}$, the scaled Stokes wave height $H/\lambda$ and the Stokes wave velocity $c$. Values of $H/\lambda$ are also encoded in the names of `.dat`-files. Also the file `summary.txt` provides a summary of the results from all `.dat`-files.

| $k$ | $\chi_k$ | $\gamma_k$ |
|---|---|---|
| 1 | 9.9604109260633508386299274610866 1e-01 | 7.8695526779881577989694097538473 0e-03 |
| 2 | 9.7897292508754451728885175500549 8e-01 | 1.5893820864998954997022015600755 8e-02 |
| 3 | 9.4956960391898253443461132765958 8e-01 | 2.0927047791466606746276244495781 3e-02 |
| 4 | 9.1040611867876780101188402299837 1e-01 | 2.3077285530923277492192703297859 3e-02 |
| 5 | 8.6469476884402377584931829263270 6e-01 | 2.2782182339553561629928246745401 4e-02 |
| 6 | 8.1578439264496778826437090223903 1e-01 | 2.0678156933425089832258207361704 2e-02 |
| 7 | 7.6677451880446474711121113328693 6e-01 | 1.7450501829186839066720197654986 2e-02 |
| 8 | 7.2028390120678522059528141797906 8e-01 | 1.3719151862055527038705285558786 8e-02 |
| 9 | 6.7836542041312713075105714170534 2e-01 | 9.7903489393458824811047018470610 e-03 |
| 10 | 6.4252748479084196766158547723149 6e-01 | 6.5873994460011043840339426702420 5e-03 |
| 11 | 6.1381466776506956201298570201429 2e-01 | 3.7802262093600304203639061879249 1e-03 |
| 12 | 5.9290831577423157102010207841802 8e-01 | 1.7006843891665575868056166496925 1e-03 |
| 13 | 5.8022088263929537210440261304535 7e-01 | 4.2793953619199851189800517724089 5e-04 |

TABLE 1. Data for Padé approximation of the wave with velocity $c = 1.005$, the steepness $H/\lambda = 0.031791185830078550217424174610939$, and $y_0 = -0.09481981887534422594045318294554 5$. Parameters of simulations and Padé approximation are $M = 16384$, $R(y) \simeq 3.64 \times 10^{-33}$, $err_{pade} \simeq 4.65 \times 10^{-31}$, and the smallest Fourier harmonic had value $|\hat{z}_{k_{max}}| \simeq 1.00 \times 10^{-39}$.

| $k$ | $\chi_k$ | $\gamma_k$ |
|---|---|---|
| 1 | 9.9510487744316298854328560421030e-01 | 9.8634425913775013192966081685342e-03 |
| 2 | 9.7403645379611316009981462350215e-01 | 2.0450766843292724632910023898083e-02 |
| 3 | 9.3757034809781764669377193799355e-01 | 2.7939215514151973598355171005255e-02 |
| 4 | 8.8848783756809908258393607521386e-01 | 3.2346695051450353689148486577530e-02 |
| 5 | 8.3022674501976472151335860427972e-01 | 3.4014778159425464029321685563311e-02 |
| 6 | 7.6633399299159945580430551628348e-01 | 3.3503165383978144324292110301296e-02 |
| 7 | 7.0004465438940742469879669205390e-01 | 3.1448953589682327363428565339677e-02 |
| 8 | 6.3403006262056448706162192538260e-01 | 2.8450081850105899436374519317018e-02 |
| 9 | 5.7030617503839145018247961238822e-01 | 2.4997228372805006377793904577406e-02 |
| 10 | 5.1025906752790243499980457271891e-01 | 2.1451165874825272034418476169493e-02 |
| 11 | 4.5473680391259471378568663592050e-01 | 1.8050667936866445311065909372440e-02 |
| 12 | 4.0416606309913686208018733764132e-01 | 1.4935324248873614040200287195258e-02 |
| 13 | 3.5866656967614594741671222027091e-01 | 1.2171983132221707818347322265224e-02 |
| 14 | 3.1814957608007288340281284482614e-01 | 9.7785979408782130502815064025153e-03 |
| 15 | 2.8239582144953721967102783100630e-01 | 7.7430496091429749767332417436128e-03 |
| 16 | 2.5111362491120612401300611962866e-01 | 6.0367316618075166060446235089549e-03 |
| 17 | 2.2398013688366070356524336177922e-01 | 4.6236887109425286072088970028436e-03 |
| 18 | 2.0066941016996420121403339168129e-01 | 3.4663799698411329904404640260248e-03 |
| 19 | 1.8087071572685151311776394077792e-01 | 2.5290675126137799203844081627572e-03 |
| 20 | 1.6429994613389934435690038788652e-01 | 1.7796298722551997100597343439724e-03 |
| 21 | 1.5070630718606119736027022149192e-01 | 1.1903886001234201479535849334361e-03 |
| 22 | 1.3987592330215211246386684753999e-01 | 7.3835466023091063736832919360058e-04 |
| 23 | 1.3163351788618449367882477199335e-01 | 4.0516436399706229881123587808757e-04 |
| 24 | 1.2584297566521574661109612239664e-01 | 1.7687731216873907019568385614406e-04 |
| 25 | 1.2240733354174996603362643446337e-01 | 4.3743035302963481666199453380096e-05 |

TABLE 2. Data for Padé approximation of the wave with velocity $c = 1.051$, the steepness $H/\lambda = 0.10042675172528485854673515635249$, and $y_0 = -0.25732914098527682158156915646871$. Parameters of simulations and Padé approximation are $M = 16384$, $R(y) \simeq 5.19 \times 10^{-32}$, $err_{pade} \simeq 1.69 \times 10^{-31}$, and the smallest Fourier harmonic had value $|\hat{z}_{k_{max}}| \simeq 1.00 \times 10^{-37}$.

| $k$ | $\chi_k$ | $\gamma_k$ |
|---|---|---|
| 1 | 9.95433825932608550132384034857213e-01 | 9.06513968659594263994154983859022e-03 |
| 2 | 9.75720732729872361661639075445556e-01 | 1.88104172479867625607988377665013e-02 |
| 3 | 9.41458580699036796998398974950063e-01 | 2.58024268240062770737774505111002e-02 |
| 4 | 8.95072079198109934865810125596955e-01 | 3.00760315302764871790369706833779e-02 |
| 5 | 8.39603368860036006278810820983949e-01 | 3.19167851791100543244698807489031e-02 |
| 6 | 7.78246707846125864530269738095348e-01 | 3.17900776761535529310595879964877e-02 |
| 7 | 7.13977463595480003911919153327480e-01 | 3.02335467307095385878230877915997e-02 |
| 8 | 6.49314375127269358025790723963870e-01 | 2.77625384158746106085149228773401e-02 |
| 9 | 5.86215465928989576951120366245581e-01 | 2.48107842884599707048520815911264e-02 |
| 10 | 5.26077937447751872984275728101522e-01 | 2.17068351144352237760178371853073e-02 |
| 11 | 4.69802407403950485965504029996914e-01 | 1.86762941525117699745376670289500e-02 |
| 12 | 4.17886269376110040045868819592273e-01 | 1.58579969144004349124961258254260e-02 |
| 13 | 3.70521444182340763884420027666827e-01 | 1.33248510736740059585812992162263e-02 |
| 14 | 3.27682439755960213510467363606042e-01 | 1.11037283880977232781708686935009e-02 |
| 15 | 2.89198722549172239607721584343698e-01 | 9.19185285105063318623096617861130e-03 |
| 16 | 2.54810466354666195816665370686997e-01 | 7.56907825149316224628365974410675e-03 |
| 17 | 2.24209367334721589574533037466343e-01 | 6.20644453419544059242384682030945e-03 |
| 18 | 1.97067225067065397541246930106441e-01 | 5.07177162315234989673990118919696e-03 |
| 19 | 1.73055091362268451120364081334665e-01 | 4.13307962854491967554778057762908e-03 |
| 20 | 1.51855462026532436104149361379210e-01 | 3.36050786167674783997799826083550e-03 |
| 21 | 1.33169515540203788156642166906591e-01 | 2.72724894316322072325277221844458e-03 |
| 22 | 1.16720933274701291000887725539493e-01 | 2.20986855953690886419588367706623e-03 |
| 23 | 1.02257431405919038178275031736290e-01 | 1.78826390264321999398279771128206e-03 |
| 24 | 8.95508127283858594116407019601820e-02 | 1.44542657328550726857080252749622e-03 |
| 25 | 7.83961028319930614767173088020279e-02 | 1.16711442195804019558665126539427e-03 |
| 26 | 6.86101566854466616210976539289158e-02 | 9.41495432894175937842874927421205e-04 |
| 27 | 6.00299941184905270702652324982135e-02 | 7.58799737152752549854592147665995e-04 |
| 28 | 5.25110331386998700818247974509258e-02 | 6.10998699362372783997691390696487e-04 |
| 29 | 4.59253281231247667007365599867943e-02 | 4.91519483298208817983041233383980e-04 |
| 30 | 4.0159877796588826715919995477710e-02 | 3.94997269772740759120747730149340e-04 |
| 31 | 3.51150396988382900972228874525109e-02 | 3.17063815302569437242780768838413e-04 |
| 32 | 3.07030693071633025856068326424687e-02 | 2.54169263655189066241987434556100e-04 |
| 33 | 2.68467901323811952321185618074578e-02 | 2.03433380026332773186591672337583e-04 |
| 34 | 2.34783937316708681288640025635146e-02 | 1.62522237707382077096302354822532e-04 |
| 35 | 2.05383642178678839200647846555908e-02 | 1.29546576264629788075276452826328e-04 |
| 36 | 1.79745193852614117777103084010265e-02 | 1.02978399018687148172885868196623e-04 |
| 37 | 1.57411593704806090331919997928406e-02 | 8.15827862763857084235776103594481e-05 |
| 38 | 1.37983133839445750806859736203507e-02 | 6.43623147351034758281773572995289e-05 |
| 39 | 1.21110752013028358188007191935072e-02 | 5.05118646282732166085507134151195e-05 |
| 40 | 1.06490185910779922966530559824050e-02 | 3.93819507325944359184298112513636e-05 |
| 41 | 9.38568452652012956402075369290278e-03 | 3.04490256349179913250724576956079e-05 |
| 42 | 8.29813278439420925351354881096343e-03 | 2.32914730544885187107604807304053e-05 |
| 43 | 7.36655130339489438745177566237321e-03 | 1.75702379530898436181417357806391e-05 |
| 44 | 6.57391741813790189283510916305043e-03 | 1.30132325361793585312305562950935e-05 |
| 45 | 5.90570578080460414802523913159400e-03 | 9.40281755981180973510534726928533e-06 |
| 46 | 5.34963842759485046283496838777743e-03 | 6.56579130822932954380944114441017e-06 |
| 47 | 4.89547304507788970804144262729396e-03 | 4.36542870899759471322771653831421e-06 |
| 48 | 4.53482604688247134485690783763108e-03 | 2.69520431445801848314129686051970e-06 |
| 49 | 4.26102758786433892841273275905455e-03 | 1.47390871215592819437170943388163e-06 |
| 50 | 4.06900612679011263031777402788905e-03 | 6.41931271126488105657466176599801e-07 |
| 51 | 3.95520060861743412410650474994064e-03 | 1.58535598642490907942230532511450e-07 |

TABLE 3. Data for Padé approximation of the wave with velocity $c = 1.0929$, the steepness $H/\lambda = 0.13825830866311310404416736817381$, and $y_0 = -0.29153391724312882929999965032009$. Parameters of simulations and Padé approximation are $M = 65536$, $R(y) \simeq 2.59 \times 10^{-31}$, $err_{pade} \simeq 1.01 \times 10^{-32}$, and the smallest Fourier harmonic had value $|\hat{z}_{k_{max}}| \simeq 5.00 \times 10^{-38}$.

| $k$ | $\chi_k$ | $\gamma_k$ |
|---|---|---|
| 1 | 9.93398643583003025153415435504531e-01 | 1.28741415762741679346145664996829e-02 |
| 2 | 9.650604820586669453480870980252106e-01 | 2.60267721567181859054226183119919e-02 |
| 3 | 9.16714789789161849202896809849705e-01 | 3.43697679627825352269776411757291e-02 |
| 4 | 8.53133231672953078297597841861823e-01 | 3.81940153445550033591099941584920e-02 |
| 5 | 7.79861194757267505357891461462460e-01 | 3.83579555843352602595202964927154e-02 |
| 6 | 7.02176870736814955937036169062899e-01 | 3.59774931820106663192752740784546e-02 |
| 7 | 6.2443191001354564111933110534714e-01 | 3.21282856711997437340001627375168e-02 |
| 8 | 5.49795332847499273525022520666518e-01 | 2.76691730121067711930378384900232e-02 |
| 9 | 4.80296232546974823630387324524545e-01 | 2.31906560517515347893552651709825e-02 |
| 10 | 4.17024645857800791824977075950470e-01 | 1.90429324287558759377242844714520e-02 |
| 11 | 3.60378305224974615221811203424356e-01 | 1.53959152585563261217878597243142e-02 |
| 12 | 3.10289842646985418345605736936048e-01 | 1.23006351687210032636876990145911e-02 |
| 13 | 2.66407648286693861932841258994721e-01 | 9.73852232172353639036354649203610e-03 |
| 14 | 2.28226886286517332438415939592608e-01 | 7.65583101348162009153247587551195e-03 |
| 15 | 1.95177843545134733789119725180096e-01 | 5.9853517004412731114464478095979e-03 |
| 16 | 1.66681805023593130823224346797399e-01 | 4.65887488461708640776107914945203e-03 |
| 17 | 1.42183993584453030868317439497003e-01 | 3.61357577121517253016005783742974e-03 |
| 18 | 1.21171172484979583446779037786714e-01 | 2.79470260489814969664959294926652e-03 |
| 19 | 1.03179452511723992079582272565214e-01 | 2.15617836676118577227243251241331e-03 |
| 20 | 8.77961228595568606401648108610398e-02 | 1.66012679310648786275121618740345e-03 |
| 21 | 7.46580315447597465030574978595406e-02 | 1.27592107645668605269203574613739e-03 |
| 22 | 6.34481306443940719507463127666211e-02 | 9.79089087450639485345366472519338e-04 |
| 23 | 5.38911872290903942028496746096495e-02 | 7.50248095624531518737269429111365e-04 |
| 24 | 4.57492587887819300483008251206986e-02 | 5.74148509163471182463355721181721e-04 |
| 25 | 3.88172752742240105088258746631741e-02 | 4.38854383779301056123215099079188e-04 |
| 26 | 3.29189096590597195144947958198357e-02 | 3.35061475940689863018834966768472e-04 |
| 27 | 2.79028212558501660025568098114343e-02 | 2.55540871176311150876065830758264e-04 |
| 28 | 2.36392981742008042750164949870111e-02 | 1.94691329540109355414952726522057e-04 |
| 29 | 2.00172924085211268884110103807234e-02 | 1.48182722053010736525844218770677e-04 |
| 30 | 1.69418235041002160106748854919734e-02 | 1.126741551887716015725439641392e-04 |
| 31 | 1.43317184931477833930656499987995e-02 | 8.55924207962470484084537963575900e-05 |
| 32 | 1.21176530092033068365142201489852e-02 | 6.49586463790799447674548874436684e-05 |
| 33 | 1.02404588173178159766150762312400e-02 | 4.92531498561398293539370127249816e-05 |
| 34 | 8.64966499042977177325090332415729e-03 | 3.73103914016284265439688122490895e-05 |
| 35 | 7.30224274879133050003140619052446e-03 | 2.82375225733516039477667066021446e-05 |
| 36 | 6.16152705009717845830463720403643e-03 | 2.13513661747602139469739101816769e-05 |
| 37 | 5.19629108350495067218636168760723e-03 | 1.61297466879220448079982238240246e-05 |
| 38 | 4.3799527229709430520221610919454e-03 | 1.21739653477311336991048098474804e-05 |
| 39 | 3.68989465744363535075551189083628e-03 | 9.17991094830884893227377698101798e-06 |
| 40 | 3.10688231013106004394611827804953e-03 | 6.91584935818872179036239759592572e-06 |
| 41 | 2.61456578557885722141496603598660e-03 | 5.20536938490202499152488268561648e-06 |
| 42 | 2.19905395393225001547396749458147e-03 | 3.91430351823738560080383189178292e-06 |
| 43 | 1.84855041619759608964615915855160e-03 | 2.94070847979427725012698794615673e-06 |
| 44 | 1.55304251639257745230445095694940e-03 | 2.20719808861136536998364371692094e-06 |
| 45 | 1.30403580024761683344961061119599e-03 | 1.65508232204597074734186170013816e-06 |
| 46 | 1.09432738764763509113618247317394e-03 | 1.23989163441506187230543611758337e-06 |
| 47 | 9.17812647645417749658202151298786e-04 | 9.27962520159008244607471765496508e-07 |
| 48 | 7.69320359699922614599799922262156e-04 | 6.93853226000040035242065190155287e-07 |
| 49 | 6.44472229750674596638565661872796e-04 | 5.18272340903010891482796683060429e-07 |
| 50 | 5.39563219268408452082296554789566e-04 | 3.86751562364387865498882802928547e-07 |
| 51 | 4.51459652187210048535645581625337e-04 | 2.88320243535854856966320396641389e-07 |
| 52 | 3.77512500082907183102947952504772e-04 | 2.1472569852411868919774299181126e-07 |
| 53 | 3.15483620098192985576130479232556e-04 | 1.59755495420848083506690922212921e-07 |
| 54 | 2.63483041310020855659728424130368e-04 | 1.18737501808356300532888071897965e-07 |
| 55 | 2.19915670752623096428691515132722e-04 | 8.81613507227033650558982811933814e-08 |

| $k$ | $\chi_k$ | $\gamma_k$ |
|---|---|---|
| 56 | 1.8343602661721882759256502530580e-04 | 6.5392105851316514611826585435320e-08 |
| 57 | 1.5290980878940366433478152173416e-04 | 4.8453871613360395138824778943192e-08 |
| 58 | 1.2738129049261870731870578892286e-04 | 3.5866415896431116145911823686790e-08 |
| 59 | 1.0604566343040422354593145915710e-04 | 2.6521934583088737099154065974285e-08 |
| 60 | 8.8225596062309732893804729077238e-05 | 1.9592183302636036836181687924269e-08 |
| 61 | 7.3351373558224491746359567216134e-05 | 1.4458560339343284528096546075837e-08 |
| 62 | 6.0944081102008910735943838284993e-05 | 1.0659519375709383139015605793475e-08 |
| 63 | 5.0601371801084779510334400335530e-05 | 7.8510551006106334507583137996502e-09 |
| 64 | 4.1985428484288675723575634713219e-05 | 5.7770409455158432066830595378940e-09 |
| 65 | 3.4812786788714960359869564796137e-05 | 4.2469845565673477161350861920841e-09 |
| 66 | 2.8845736534482650253967071944154e-05 | 3.1193627269584669263303161388805e-09 |
| 67 | 2.3885060701563551072991988129380e-05 | 2.2891489600802587729342558367170e-09 |
| 68 | 1.9763907437738515507152157402248e-05 | 1.6784884233609680030238490069172e-09 |
| 69 | 1.6342621328360279425835697021146e-05 | 1.2297332911535108807690802781445e-09 |
| 70 | 1.3504386390917315650033881549445e-05 | 9.0024649439482668776624110382357e-10 |
| 71 | 1.1151555586215682493972231695178e-05 | 6.5852901813774357346449810625888e-10 |
| 72 | 9.2025606417064019824688878568765e-06 | 4.8133677942506421965934875135458e-10 |
| 73 | 7.5893121361235946296571640618554e-06 | 3.5153662296011708064897275385769e-10 |
| 74 | 6.2550134916523302541644726635149e-06 | 2.5651378901198414024451439118085e-10 |
| 75 | 5.1523240917958044222360736326013e-06 | 1.8699041153184304677867073872509e-10 |
| 76 | 4.2418164977501652292770967858889e-06 | 1.3615002707058387759820737340000e-10 |
| 77 | 3.4906810681295210983466572203766e-06 | 9.8989612553651394882089479387058e-11 |
| 78 | 2.8716387090428197812338112049988e-06 | 7.1840549795176352444815094831865e-11 |
| 79 | 2.3620292727864461413493859288553e-06 | 5.2014866582954146275639907961284e-11 |
| 80 | 1.9430488528549484390946676753357e-06 | 3.7544371994904332049108108901540e-11 |
| 81 | 1.5991132106501738064175343479085e-06 | 2.6988677125981984704746234222767e-11 |
| 82 | 1.3173271524016967143347779633334e-06 | 1.9294191393489425054514424415497e-11 |
| 83 | 1.0870421146965101702321081549869e-06 | 1.3690682657345570830587734041507e-11 |
| 84 | 8.9948710302840591107924047505277e-07 | 9.6154320453706342539025316603398e-12 |
| 85 | 7.4746094473483549460315060568125e-07 | 6.6576551472015402342820220083834e-12 |
| 86 | 6.2507601280318307294971499677821e-07 | 4.5178196858914743568166113879862e-12 |
| 87 | 5.2754518840784040403497240236470e-07 | 2.9779080579673535305615806385976e-12 |
| 88 | 4.5100527954754306951284004525927e-07 | 1.8797051053782461474158871160223e-12 |
| 89 | 3.9237196672768684765242246013712e-07 | 1.1089624254962664338566606478705e-12 |
| 90 | 3.4922420693522630789517260741251e-07 | 5.8390168187016781680289381142924e-13 |
| 91 | 3.1971991332090189389755215991650e-07 | 2.4705505284211588975522964996134e-13 |
| 92 | 3.0254732567911305773280626530688e-07 | 5.9906268082502519128433486646726e-14 |

TABLE 4. Data for Padé approximation of the wave with velocity $c = 1.0922851405$, the steepness $H/\lambda = 0.14105777885488320816492860225696$, and $y_0 = -0.28978481161845687297742961144$. Parameters of simulations and Padé approximation are $M = 134217728$, $R(y) \simeq 6.14 \times 10^{-27}$, $err_{pade} \simeq 5.43 \times 10^{-27}$, and the smallest Fourier harmonic had value $|\hat{z}_{k_{max}}| \simeq 3.00 \times 10^{-31}$.

REFERENCES

ALPERT, BRADLEY, GREENGARD, LESLIE & HAGSTROM, THOMAS 2000 Rapid evaluation of nonreflecting boundary kernels for time-domain wave propagation. *SIAM J. Num. Anal.* **37**, 1138–1164.

AMICK, C. J., FRAENKEL, L. E. & TOLAND, J. F. 1982 On the stokes conjecture for the wave of extreme form. *Acta Math.* **148**, 193–214.

APTEKAREV, A. I., BUSLAEV, V. I., MARTINEZ-FINKELSHTEIN, A. & SUETIN, S.P. 2011 Padé approximants, continued fractions, and orthogonal polynomials. *Russian Math. Surveys* **88**, 1049–1131.

BAKER, GREGORY R. & XIE, CHAO 2011 Singularities in the complex physical plane for deep water waves. *J. Fluid Mech.* **685**, 83–116.

DE MONTESSUS DE BALLORE, R. 1902 Sur les fractions continues algébriques. *Bull. Soc. Math. France* **30**, 28–36.

BUSLAEV, V. I. 2001 Simple counterexample to the baker-gammel-wills conjecture. *East J. Approx.* **7**, 515–517.

CHEN, B & SAFFMAN, PG 1980 Numerical evidence for the existence of new types of gravity-waves of permanent form on deep-water. *Studies in Applied Mathematics* **62** (1), 1–21.

COWLEY, STEPHEN J., BAKER, GREG R. & TANVEER, SALEH 1999 On the formation of moore curvature singularities in vortex sheets. *J. Fluid Mech.* **378**, 233–267.

DRENNAN, W.M., HUI, W.H. & TENTI, G. 1992 Accurate calculations of stokes water waves of large amplitude. *Zeitschrift fur angewandte Mathematik und Physik ZAMP* **43** (2), 367–384.

DYACHENKO, ALEXANDER I., KUZNETSOV, EVGENII A., SPECTOR, MICHAEL & ZAKHAROV, VLADIMIR E. 1996*a* Analytical description of the free surface dynamics of an ideal fluid (canonical formalism and conformal mapping). *Phys. Lett. A* **221**, 73–79.

DYACHENKO, A. I., ZAKHAROV, V. E. & KUZNETSOV, E. A. 1996*b* Nonlinear dynamics of the free surface of an ideal fluid. *Plasma Physics Reports* **22**, 829–840.

DYACHENKO, SERGEY A., LUSHNIKOV, PAVEL M. & ALEXANDER O. KOROTKEVICH, HTTP://STOKESWAVE.ORG 2015 .

DYACHENKO, SERGEY A., LUSHNIKOV, PAVEL M. & KOROTKEVICH, ALEXANDER O. 2013 The complex singularity of a stokes wave. *JETP Letters* **98** (11), 767–771.

FRIGO, MATEO & JOHNSON, STEVEN G. 2005 The design and implementation of fftw 3, http://fftw.org. *Proc. IEEE* **93** (2), 216–231.

G. A. BAKER, JR. & GRAVES-MORRIS, P. R. 1996 *Padé Approximants, 2nd ed.,*. Cambridge: Cambridge Univ. Press.

GAKHOV, F. D. 1966 *Boundary Value Problems*. New York: Pergamon Press.

GANDZHA, I. S. & LUKOMSKY, V. P. 2007 On water waves with a corner at the crest. *Proc. R. Soc. A* **463**, 1597.

GNU PROJECT, HTTP://GNU.ORG 1984-2012 .

GONCHAR, A. A. 1973 On the convergence of padé approximants. *Math. USSR Sb.* **21**, 155–166.

GONCHAR, A. A. 1975 On the convergence of generalized padé approximants of meromorphic functions. *Math. USSR Sb.* **27**, 503–514.

GONNET, PEDRO, PACHON, RICARDO & TREFETHEN, LLOYD N. 2011 Robust rational interpolation and least-squares. *Electronic Transactions on Numerical Analysis* **1388**, 146–167.

GRANT, MALCOLM A. 1973 The singularity at the crest of a finite amplitude progressive stokes wave. *J. Fluid Mech.* **59(2)**, 257–262.

HESTENES, MAGNUS R. & STIEFEL, EDUARD 1952 Methods of conjugate gradients for solving linear systems. *J. Research of Nat. Bureau of Standards* **49** (6), 409–436.

INOGAMOV, N. A. & OPARIN, A. M. 2003 Bubble motion in inclined pipes. *Journal of Experimental and Theoretical Physics* **97**, 1168–1185.

KUZNETSOV, E.A., SPECTOR, M.D. & ZAKHAROV, V.E. 1993 Surface singularities of ideal fluid. *Physics Letters A* **182** (4-6), 387 – 393.

KUZNETSOV, E. A., SPECTOR, M. D. & ZAKHAROV, V. E. 1994 Formation of singularities on the free surface of an ideal fluid. *Phys. Rev. E* **49**, 1283–1290.

LAKOBA, TARAS I. & YANG, J. 2007 A generalized petviashvili iteration method for scalar and

vector hamiltonian equations with arbitrary form of nonlinearity. *J. Comput. Phys.* **226**, 1668–1692.

LAU, S. R. 2004 Rapid evaluation of radiation boundary kernels for time-domain wave propagation on blackholes: implementation and numerical tests. *Class. Quantum Grav* **21**, 4147–4192.

LONGUET-HIGGINS, MICHAEL S. 2008 On an approximation to the limiting stokes wave in deep water. *Wave Motion* **45**, 770–775.

LONGUET-HIGGINS, M. S. & FOX, M. J. H. 1977 Theory of the almost-highest wave: the inner solution. *J. Fluid Mech.* **80(4)**, 721–741.

LONGUET-HIGGINS, M. S. & FOX, M. J. H. 1978 Theory of the almost-highest wave. part 2. matching and analytic extension. *J. Fluid Mech.* **85(4)**, 769–786.

LUBINSKY, D. S. 2003 Rogers-ramanujan and the baker-gammel-wills (padé) conjecture. *Ann. of Math.* **157**, 847–889.

LUENBERGER, DAVID G. 1970 The conjugate residual method for constrained minimization problems. *SIAM J. Numer. Anal.* **7** (3), 390–398.

LUSHNIKOV, P. M. 2001 Dispersion-managed soliton in a strong dispersion map limit. *Opt. Lett.* **26**, 1535 – 1537.

LUSHNIKOV, P. M. 2004 Exactly integrable dynamics of interface between ideal fluid and light viscous fluid. *Physics Letters A* **329**, 49 – 54.

MARKOFF, A. 1895 Deux démonstrations de la convergence de certaines fractions continues. *Acta Math.* **19**, 93–104.

MEISON, D., ORZAG, S. & IZRAELY, M. 1981 Applications of numerical conformal mapping. *J. Comput. Phys.* **40**, 345–360.

MICHELL, JOHN H. 1893 The highest waves in water. *Phil. Mag. Series 5* **36**, 430–437.

MINEEV-WEINSTEIN, MARK, WIEGMANN, PAUL B & ZABRODIN, ANTON 2000 Integrable structure of interface dynamics. *Physical Review Letters* **84** (22), 5106–5109.

MOORE, D. W. 1979 The spontaneous appearance of a singularity in the shape of an evolving vortex sheet. *Proceedings of the Royal Society of London A: Mathematical, Physical and Engineering Sciences* **365** (1720), 105–119.

NEKRASOV, ALEKSANDR I. 1921 On steady waves. *Izv. Ivanovo-Voznesensk. Polytech. Inst.* **3**, 52–56.

NEKRASOV, ALEKSANDR I. 1951 *The exact theory of standing waves on the surface of heavy fluid*. Moscow: Izdat. Akad. Nauk. SSSR.

NUTTALL, J. 1970 The convergence of padé approximants of meromorphic functions. *J. Math. Anal. Appl.* **31**, 147–153.

OVSYANNIKOV, LEV V. 1973 Dynamics of a fluid. *M.A. Lavrent'ev Institute of Hydrodynamics Sib. Branch USSR Ac. Sci.* **15**, 104–125.

PELINOVSKY, D.E. & STEPANYANTS, YU.A. 2004 Convergence of petviashvili's iteration method for numerical approximation of stationary solutions of nonlinear wave equations. *SIAM J. Numer. Anal.* **42**, 1110–1127.

PETVIASHVILI, VLADIMIR I. 1976 Equation for an extraordinary soliton. *Sov. J. Plasma Phys.* **2**, 257–258.

PLOTNIKOV, P.I. 1982 A proof of the stokes conjecture in the theory of surface waves. *Dinamika Splosh. Sredy (In Russian. English translation Stud. Appl. Math.3, 217-244 (2002))* **57**, 41–76.

POLYANIN, ANDREI D. & MANZHIROV, ALEXANDER V. 2008 *Handbook of Integral Equations: Second Edition*. Boca Raton: Chapman and Hall/CRC.

RAINEY, R. C. T. & LONGUET-HIGGINS, MICHAEL S. 2006 A close one-term approximation to the highest stokes wave on deep water. *Ocean Engineering* **33**, 2012–2024.

SAFF, E. B. 1972 An extension of montessus de ballore's theorem on the convergence of interpolating rational functions. *J. Approximation Theory* **6**, 63–67.

SCHWARTZ, LEONARD W. 1974 Computer extension and analytic continuation of stokes' expansion for gravity waves. *J. Fluid Mech.* **62(3)**, 553–578.

SRETENSKII, LEONID N. 1976 *Theory of wave motion of fluid*. Moscow: Nauka.

STAHL, H. 1985*a* Extremal domains associated with an analytic function, i. *Complex Variables Theory Appl.* **4**, 311–324.

STAHL, H. 1985*b* Extremal domains associated with an analytic function, ii. *Complex Variables Theory Appl.* **4**, 321–338.

STAHL, H. 1997 The convergence of padé approximants to functions with branch points. *J. Approx. Theory* **91**, 139–204.

STOKES, GEORGE G. 1847 On the theory of oscillatory waves. *Transactions of the Cambridge Philosophical Society* **8**, 441–455.

STOKES, GEORGE G. 1880*a* On the theory of oscillatory waves. *Mathematical and Physical Papers* **1**, 197–229.

STOKES, GEORGE G. 1880*b* Supplement to a paper on the theory of oscillatory waves. *Mathematical and Physical Papers* **1**, 314–326.

TANVEER, S. 1991 Singularities in water waves and rayleigh-taylor instability. *Proc. R. Soc. Lond. A* **435**, 137–158.

TANVEER, S. 1993 Singularities in the classical rayleigh-taylor flow: formation and subsequent motion. *Proc. R. Soc. Lond. A* **441**, 501–525.

TOLAND, J. F. 1978 On the existence of a wave of greatest height and stokes's conjecture. *Proc. R. Soc. Lond. A* **363**, 469–485.

TURITSYN, S. K., LAI, L., & ZHANG, W. W. 2009 Asymmetric disconnection of an underwater air bubble: Persistent neck vibrations evolve into a smooth contact. *Phys. Rev. Lett.* **103**, 124501.

WILLIAMS, J. M. 1981 Limiting gravity waves in water of finite depth. *Phil. Trans. R. Soc. Lond. A* **302(1466)**, 139–188.

WILLIAMS, JOHN M 1985 *Tables of Progressive Gravity Waves*. London: Pitman.

WU, S. 2009 Almost global wellposedness of the 2-d full water wave problem. *Invent. Math* **177**, 45–135.

WU, S. 2011 Global wellposedness of the 3-d full water wave problem. *Invent. Math* **184**, 125–220.

YANG, JIANKE 2009 Newton-conjugate-gradient methods for solitary wave computations. *J Comput. Phys.* **228(18)**, 7007–7024.

YANG, JIANKE 2010 *Nonlinear Waves in Integrable and Nonintegrable Systems*. SIAM.

ZAKHAROV, VLADIMIR E. 1968 Stability of periodic waves of finite amplitude on a surface. *J. Appl. Mech. Tech. Phys.* **9** (2), 190–194.

ZAKHAROV, V. E., DYACHENKO, A. I. & PROKOFIEV, A. O. 2006 Freak waves as nonlinear stage of stokes wave modulation instability. *European Journal of Mechanics B/Fluids* **25**, 677–692.

ZAKHAROV, VLADIMIR E., DYACHENKO, ALEXANDER I. & VASILIEV, OLEG A. 2002*a* New method for numerical simulation of a nonstationary potential flow of incompressible fluid with a free surface. *Eur. J. Mech. B/Fluids* **21**, 283–291.

ZAKHAROV, VLADIMIR E., DYACHENKO, ALEXANDER I. & VASILIEV, OLEG A. 2002*b* New method for numerical simulation of nonstationary potential flow of incompressible fluid with a free surface. *European Journal of Mechanics B/Fluids* **21**, 283–291.

ZAKHAROV, VLADIMIR E., KOROTKEVICH, ALEXANDER O. & PROKOFIEV, ALEXANDER O. 2009 On dissipation function of ocean waves due to whitecapping. *AIP Proceedings, CP1168* **2**, 1229–1231.

ZAKHAROV, VLADIMIR E., KOROTKEVICH, ALEXANDER O., PUSHKAREV, ANDREI & RESIO, DONALD 2007 Coexistence of weak and strong wave turbulence in a swell propagation. *Phys. Rev. Lett.* **99** (16), 164501.